JOURNAL OF PETROLOGY | VOLUME 45 | NUMBER 2 | PAGES 321–341 | 2004 | DOI: 10.1093/petrology/egg098

Contrasting Enrichments in High- and Low-Temperature Mantle Xenoliths from Nushan, Eastern China: Results of a Single Metasomatic Event during Lithospheric Accretion?

YI-GANG XU[1]* AND JEAN-LOUIS BODINIER[2]

[1]GUANGZHOU INSTITUTE OF GEOCHEMISTRY, CHINESE ACADEMY OF SCIENCES, 510640 WUSHAN, GUANGZHOU, P.R. CHINA

[2]LABORATOIRE DE TECTONOPHYSIQUE, ISTEEM, UMR 5568, CC 49, CNRS AND UNIVERSITÉ MONTPELLIER 2, 34095 MONTPELLIER, FRANCE

RECEIVED NOVEMBER 13, 2002; ACCEPTED AUGUST 8, 2003

Distinct equilibration temperatures, deformation and trace element characteristics are observed in amphibole-bearing and amphibole-free peridotite xenoliths from Nushan, Sino-Korean Craton, eastern China. Amphibole-free peridotites are predominantly deformed, fine-grained (~1 mm) and equilibrated at 990–1110°C. Their cpx are characterized by either light rare earth element (LREE)-depleted or relatively flat REE patterns with only a slight depletion in high field strength elements (HFSE). LREE enrichment is generally associated with Fe-rich samples, consistent with 'wall-rock' metasomatism adjacent to basaltic veins. In contrast, amphibole-bearing peridotites are less deformed, coarse-grained (>3 mm) and display chemical zonation in the pyroxenes suggesting cooling from 1050 to 850°C. Their cpx show a large variation in LREE (Ce_n = 1·7–68) and almost constant heavy rare earth element (HREE) contents (Yb_n = 9·8–11·6). The highest LREE contents occur in cpx from amphibole-rich samples, coupled with Fe enrichment, strong enrichment in Th and U, and marked depletion in the HFSE. These characteristics may be accounted for by combined 'wall-rock' and 'diffuse' metasomatism involving an agent rich in volatiles and incompatible elements. As such the Nushan xenoliths could represent samples from two spatially separate metasomatic aureoles. Conversely, the cryptic and modal metasomatism could be genetically related, because the amphibole-peridotites and Fe-rich amphibole-free samples show similar Sr–Nd isotopic ranges that are indistinguishable from those of the Cenozoic basalts from eastern China. The different metasomatic assemblage and the trace element composition can be accounted for in terms of P–T *control on amphibole stability and progressive chemical evolution of asthenosphere-derived melts during upward migration. Trace element signatures and metasomatic assemblages, together with the fertile composition of the Nushan peridotites, suggest an origin as newly accreted lithosphere rather than as relic cratonic mantle. Metasomatism may have occurred after late Mesozoic lithospheric thinning, which marked a dramatic change in lithospheric architecture beneath the Sino-Korean Craton.*

KEY WORDS: *mantle; metasomatism; peridotite xenoliths; thermal evolution; trace element geochemistry; Sino-Korean Craton*

INTRODUCTION

Among the mantle xenolith localities in eastern China, the Nushan Quaternary volcanic cone in Anhui province attracts much attention because it carries abundant mantle xenoliths, which are extremely varied in their mineralogy and texture. Mantle xenoliths including amphibole-bearing and amphibole-free spinel lherzolites, garnet-bearing lherzolites and pyroxenites have been documented at this single locality (Zhang &

*Corresponding author. Telephone: 86 20 85290109. Fax: 86 20 85290130. E-mail: yigangxu@gig.ac.cn

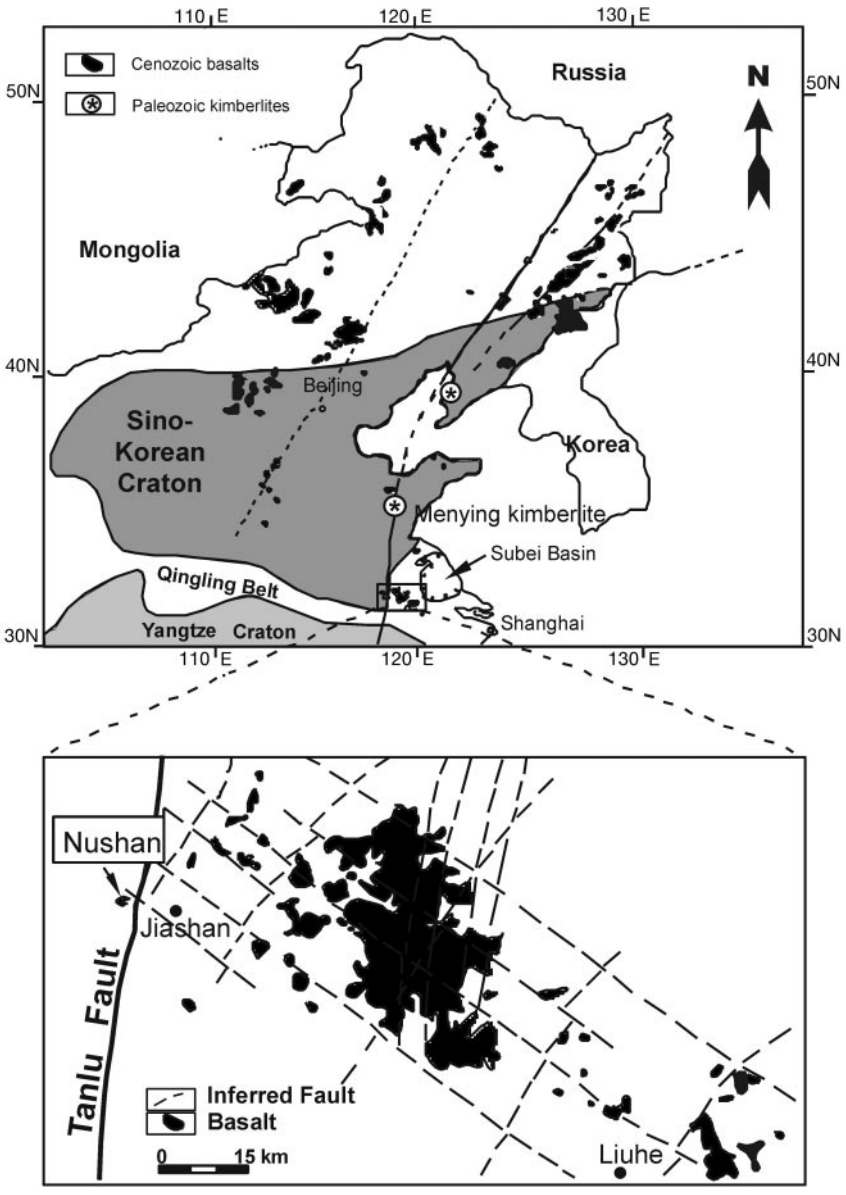

Fig. 1. A sketch map showing the simplified tectonic framework of eastern China and the location of the studied area [modified after E & Zhao (1987)].

Cong, 1987; Xu *et al*., 1997, 1998*a*). Such a broad spectrum of rock types provides a good opportunity for studying mantle stratigraphy, the thermal state of the lithosphere and mantle enrichment processes. In addition, Nushan is located at the southern edge of the Archaean Sino-Korean Craton, where both Palaeozoic diamondiferous kimberlites and Cenozoic basalts have erupted (Fig. 1). Previous studies have revealed a significant change in the thermal gradient within the lithosphere from the Palaeozoic ($\sim$40 mW/m^2) to the Cenozoic (>80 mW/m^2) (Griffin *et al*., 1998; Menzies & Xu, 1998). The present lithospheric thickness in this region is 80–100 km (Chen *et al*., 1991), significantly thinner than estimates for the Palaeozoic lithosphere (>200 km). This has led to the proposition that the mantle lithosphere beneath the Sino-Korean Craton has been significantly thinned (Menzies *et al*., 1993; Griffin *et al*., 1998). Accompanying lithospheric thinning, the upper mantle evolved from an initially refractory protolith (predominantly harzburgite) to more fertile compositions (lherzolite) (Menzies *et al*., 1993; Griffin *et al*., 1998). Mantle xenoliths from this locality

are therefore crucial in understanding the nature of the mantle in this region (old lithospheric relict versus newly accreted mantle) and processes associated with lithospheric thinning and accretion.

Previous studies concentrated on construction of palaeogeotherms and the composition of the lithospheric mantle (Xu *et al*., 1998*a*, 2000). In this contribution, attention is focused on petrological and geochemical comparisons between amphibole-bearing and amphibole-free spinel peridotites. Based on electron microprobe and inductively coupled plasma-mass spectrometry (ICP-MS) data, it will be shown that these two groups record distinct temperature regimes and display significantly different deformation and trace element characteristics. These data are integrated to define the mechanism and source of mantle metasomatism, to explore the relationship between cryptic and modal metasomatism and to further characterize the temperature–deformation relationship in the upper mantle beneath this region (Xu *et al*., 1998*b*). Finally, we place the observations within the regional geodynamic framework to understand the evolution of the lithosphere beneath the craton.

PETROGRAPHY

The Nushan volcanic crater is located within the southern part of the Tanlu Fault and at the periphery of the Jiashan–Liuhe volcanic complex (Fig. 1). Mantle xenoliths are found in both basaltic flows and scoria. No correlation is observed between the texture/petrography of the xenoliths and their mode of occurrence. Spinel peridotites are the dominant xenoliths at Nushan although rare garnet-bearing xenoliths are also found (Xu *et al*., 1998*a*). They range in size from a few centimetres to over 40 cm. The samples studied in this work can be classified into two groups in terms of the presence or absence of amphibole (Table 1). Using the textural classification of Mercier & Nicolas (1975), we can distinguish three textural types that are, in order of increasing degree of deformation: (1) coarse-grained protogranular; (2) porphyroclastic; (3) tabular equigranular. The amphibole-bearing and amphibole-free peridotites tend to show different microstructures (Table 1).

Sixty-seven of the 90 xenoliths examined in thin section are amphibole-free spinel lherzolites. Modal compositions estimated by point counting are: olivine (ol) 52–62%, orthopyroxene (opx) 22–28%, clinopyroxene (cpx) 10–17% and spinel (sp) 1–2·5%, indicating a fertile–mildly depleted character for this group (see also Xu *et al*., 2000). A number of samples have a reddish appearance in hand specimen probably as a result of oxidation near the surface. In thin section, this alteration appears to be developed mainly in olivine that has been partially transformed to iddingsite (Baker & Haggerty, 1967). Various types of dislocation structures are observed in these naturally oxidized samples as a result of plastic deformation at high temperature. The dominant texture for the amphibole-free peridotites is tabular equigranular with grain size <1 mm (Mercier & Nicolas, 1975). Porphyroclastic and protogranular textures are less common (<15% of the amphibole-free samples). Sample N-34 contains coarse green cpx (>1 cm) with exsolution lamellae of opx and sp. Samples N-6 and XON-13 contain rare grains of phlogopite, but show a tabular equigranular texture identical to that in the majority of the anhydrous peridotites. For this reason, as well as their similar equilibrium temperatures and trace element signature to those of the anhydrous peridotites (see following sections), these phlogopite-bearing peridotites are grouped with the amphibole-free suite.

Twenty-one of the samples examined contain amphibole. The modal fraction of amphibole varies from rare small disseminated grains (N-24) to >5% (N-22), but most samples contain <1% amphibole (Table 1). The modal proportions of other minerals are 55–73% ol, 16–27% opx, 7–12% cpx and 0·7–2% sp. Amphibole usually occurs as small grains surrounding brown primary spinels, or as large grains completely enclosing spinel. It also occurs either interstitially at grain boundaries or as small inclusions in large olivines. Most commonly (>90%), the amphibole-peridotites have protogranular to porphyroclastic textures, characterized by a coarse grain size (3–6 mm for ol and opx; 2–3 mm for cpx) and relatively large spinels (>2 mm). Only one amphibole-bearing sample (N-26) shows a tabular equigranular texture. Nevertheless, this sample differs in texture from the amphibole-free peridotites in having a much larger olivine grain size (0·5–1 mm × 2–5 mm). All these features suggest that the amphibole-bearing peridotites have experienced less intense deformation than the amphibole-free peridotites. Opx in amphibole-peridotites often contains fine exsolution lamellae (<5 μm) of cpx, a feature that is rarely observed in the amphibole-free group.

ANALYTICAL TECHNIQUES

Minerals were analysed for major elements with a CAMEBAX electron microprobe at University of Paris 6, using analytical conditions described by Xu *et al*. (1993). To estimate the 'bulk composition' of the pyroxene before unmixing, we have applied the integrated scanning technique normal to exsolution lamellae as described by Witt & Seck (1987). The xenoliths were sawn into slabs and the central parts were used for bulk-rock analyses and for mineral separation. The

Table 1: Petrographic characteristics and temperatures (°C) of the peridotite xenoliths from Nushan

Sample	Petrography	*T*1	*T*2	*T*3
Amphibole-free peridotites				
N-10	Porphyroclastic–equigranular (with one opx porphyroclast)	996	1059	1046
N-16	Tabular equigranular (ol: 0·5 mm × 1–1·5 mm)	1060	1083	1107
N-21	Tabular equigranular (ol: <0·5 mm × 1–1·5 mm)	1065	1076	1104
N-28	Porphyroclastic–equigranular (4 opx porphyroclast of >5 mm)	1111	1070	1043
N-34	Protogranular–porphyroclastic (with a large cpx of 1 cm)	990	987	983
N-35	Mosaic equigranular (ol: 1–2 mm)	1096	1068	1082
XON-4	Tabular equigranular (ol: <0·5 mm × 1–1·5 mm)	1045	1053	1062
XON-19	Tabular equigranular (ol: <0·5 mm × 1–1·5 mm)	1029	1035	1049
XON-50	Tabular equigranular (ol: <0·5 mm × 1–1·5 mm)	1053	1081	1100
Phlogopite-bearing lherzolites				
N-6	Tabular equigranular (ol: 0·5 mm × 1·5–2 mm)	1107	1075	1062
XON-13	Tabular equigranular			
Amphibole-bearing lherzolites				
N-11	Protogranular, am (tr.)	846	925–890	974–910
N-13	Protogranular–porphyroclastic (ol, opx: 3–5 mm), am (3·5%)	900	912–887	981–943
N-17	Porphyroclastic (ol: 3–5 mm; abundant subgrains), am (tr.)	881	1003–913	974–919
N-22	Protogranular–porphyroclastic (ol, opx: 3–5 mm), am (5%)	912	909–893	968–937
N-24	Porphyroclastic (bimodal distribution of ol grain size), am (tr.)	766	931–839	965–853
N-26	Tabular equigranular (grain size of ol: 0·5–1 mm × 2–5 mm), am (tr.)	822	887–868	922–875
N-32	Protogranular (ol: 4–8 mm; vermicular spinel), am (tr.)	860	917–900	980–881
N-37	Porphyroclastic, am (tr.)	772	1042–956	1047–922
XON-24	Protogranular, am (1·5%)			
XON-25	Protogranular, am (2·5%)			
XON-42	Protogranular–porphyroclastic, am (tr.)			
XON-45	Protogranular, am (tr.)			
XON-47	Protogranular, am (3%)			

The number following am is the modal percentage of amphibole in thin section; tr. means only a few grains of amphibole are present. *T*1, *T*2 and *T*3 are calculated using the two-pyroxene thermometer of Brey & Kohler (1990), Ca-in-opx thermometer of Brey & Kohler (1990) and Cr/Al-opx thermometer of Witt-Eickschen & Seck (1991), respectively. *T*1 values for the amphibole-bearing peridotites are calculated from the pair compositions of opx porphyroclastic rim and cpx rim. The upper and lower limits of *T*2 and *T*3 are calculated based on the compositions of porphyroclastic core and rim, respectively.

rocks were crushed in a steel mortar and ground in a carbide mill. Mineral separates were hand-picked under a binocular microscope. Cpx was leached with hot (about 100°C) 6N HCl for 45 min and then washed six times with MILLIQ pure water before acid digestion. Trace element abundances [rare earth elements (REE), Rb, Ba, U, Th, Sr, Zr, Hf, Nb and Ta] in three bulk rocks and 20 cpx separates were analysed using solution ICP-MS at Montpellier. The analytical procedure followed that described by Ionov *et al.* (1992). Blank corrections were generally small, mainly in the range 2–5% for REE and around 10% for high field strength elements (HFSE). Precision for REE and other incompatible elements is estimated to be 10% for U, Th, Nb and Ta, and better than 5% for other elements from international (PCC-1, UB-N) and internal (RO-A1) standards. Cpx separates of five samples were analysed for Sr–Nd isotopic composition at Royal Holloway University of London using published experimental procedures (Thirlwall, 1991). Analyses of standards during the period of analysis were as follows: SRM987 gave $^{87}Sr/^{86}Sr = 710245 \pm 14$ (2 SD, $n = 160$); the in-house laboratory Nd standard (low Aldrich) gave $^{143}Nd/^{144}Nd = 0{\cdot}511413 \pm 7$ (2 SD, $n = 37$), equivalent to a value of 0·511860 for the La Jolla international standard.

RESULTS

Mineral composition

Mg/(Mg + Fe) (Mg#) ratios of olivine range from 0·890 to 0·905 (Table 2a). No significant compositional

Table 2a: Representative microprobe analyses of olivine, spinel, amphibole and phlogopite from peridotite xenoliths from Nushan, astern China

	Amphibole-bearing peridotites								Ph-lherz.	Amphibole-free peridotites				
Sample:	N-11	N-13	N-17	N-22	N-24	N-26	N-32	N-37	N-6	N-10	N-21	N-28	N-34	N-35
Olivine														
SiO_2	40·12	40·28	39·84	40·39	40·16	40·47	40·30	40·72	40·34	40·00	39·96	40·57	40·39	40·16
FeO*	9·54	9·85	10·17	10·25	9·38	10·11	9·64	9·35	10·33	10·40	9·13	10·51	10·25	10·45
MgO	49·07	49·45	48·48	48·80	49·88	49·10	49·63	49·47	48·55	48·81	49·55	48·22	48·80	49·06
CaO	0·06	0·03	0·04	0·03	0·03	0·04	0·04	0·02	0·07	0·11	0·11	0·10	0·09	0·07
MnO	0·11	0·13	0·20	0·18	0·11	0·11	0·14	0·09	0·16	0·15	0·12	0·15	0·18	0·14
NiO	0·39	0·35	0·34	0·39	0·42	0·36	0·36	0·32	0·34	0·33	0·38	0·31	0·39	0·34
Total	99·31	100·12	99·12	100·04	99·99	100·25	100·14	99·98	99·86	99·84	99·34	99·96	100·04	100·29
Mg#	0·902	0·900	0·895	0·895	0·904	0·897	0·902	0·904	0·893	0·893	0·906	0·895	0·891	0·893
Spinel														
SiO_2	0·03	0·01	0·04	0·00	0·02	0·04	0·03	0·00	0·09	0·07	0·10	0·09	0·08	0·08
TiO_2	0·13	0·06	0·14	0·03	0·06	0·06	0·10	0·01	0·23	0·12	0·14	0·26	0·20	0·24
Al_2O_3	51·45	53·34	57·97	49·18	55·75	58·50	55·31	54·71	57·17	45·13	46·68	57·67	57·75	54·02
Cr_2O_3	15·27	15·50	10·55	19·80	13·62	9·90	12·42	13·83	9·46	21·25	21·10	8·57	10·03	13·10
FeO*	11·10	11·46	10·35	12·19	11·08	7·87	10·23	10·46	10·81	13·85	11·39	11·44	10·69	11·36
MgO	18·90	19·62	20·34	18·38	19·88	22·19	19·90	19·67	20·29	18·20	19·12	20·49	20·25	19·69
Total	97·28	100·43	99·82	99·99	100·87	99·02	98·50	99·07	98·54	98·98	99·00	98·93	99·46	98·90
Cr#	0·17	0·16	0·11	0·27	0·16	0·10	0·14	0·15	0·10	0·24	0·23	0·09	0·11	0·14
Mg#	0·77	0·77	0·79	0·74	0·77	0·86	0·79	0·78	0·79	0·75	0·78	0·80	0·79	0·79
Amphibole and phlogopite														
SiO_2	43·21	43·18	43·19	43·38	43·15	43·24	43·05	43·94	37·38					
TiO_2	1·87	1·17	2·49	0·95	2·85	1·46	1·84	1·69	7·00					
Al_2O_3	14·67	14·97	14·82	14·74	14·29	15·43	14·91	14·06	16·52					
Cr_2O_3	1·25	1·42	1·00	1·73	1·03	0·93	1·14	1·32	1·11					
FeO*	3·70	3·65	3·68	3·77	3·34	3·62	3·51	3·40	4·81					
MgO	17·37	17·19	17·10	17·10	17·38	17·41	17·43	18·11	18·17					
CaO	10·90	10·73	10·59	10·14	11·39	10·31	10·97	10·83	0·04					
Na_2O	3·41	3·21	3·60	3·65	3·67	4·03	3·41	3·62	0·26					
K_2O	1·08	1·57	0·66	1·11	0·16	0·14	0·91	0·30	10·06					
Total	97·62	97·79	97·28	96·72	97·38	96·81	97·32	97·50	95·53					
Cr#	0·05	0·06	0·04	0·07	0·05	0·04	0·05	0·06	0·04					
Mg#	0·894	0·894	0·893	0·891	0·904	0·896	0·899	0·906	0·872					

FeO* as total Fe.

difference was found between olivines in the amphibole-bearing peridotites and those in the amphibole-free samples, except for CaO. The latter are systematically higher in CaO (0·07–0·11 wt %) than the former (0·02–0·06 wt %).

All spinels are chromiferous with Cr/(Cr + Al) ($Cr\#_{sp}$) ranging from 0·1 to 0·3 (Table 2a). The anti-correlation between $Cr\#_{sp}$ and $Mg\#_{sp}$ (except for N-26; not shown) is identical to that defined by Dick & Bullen (1984) for abyssal peridotites. No significant difference (even for Fe^{3+}) exists between spinels from the amphibole-free and amphibole-bearing suites. The spinel in N-26 has a considerably higher Mg# at a Cr# of 0·1, compared with the compositional trend of oceanic peridotites.

Amphiboles are pargasites (Table 2a). They are compositionally similar to interstitial amphiboles in peridotite xenoliths from worldwide alkali basalts

Table 2b: Representative microprobe analyses of orthopyroxenes from peridotite xenoliths from Nushan

	Amphibole-bearing peridotites												Ph-lherz	Amphibole-free peridotites									
Sample:	N-11		N-24				N-26		N-32		N-37		N-6	N-10		N-21		N-28		N-34		N-35	
	core	rim	P core	P rim	N core	N rim	core	rim	core	rim	core	rim		core	rim	core	rim	core	rim	core	rim	core	rim
SiO_2	54·89	55·31	55·03	55·60	55·79	56·29	55·38	55·90	54·54	55·83	55·00	56·48	53·50	54·30	54·75	54·99	54·24	53·69	53·76	54·70	54·92	53·94	53·37
TiO_2	0·09	0·09	0·13	0·08	0·08	0·06	0·08	0·08	0·12	0·11	0·10	0·07	0·17	0·04	0·03	0·08	0·07	0·17	0·21	0·13	0·10	0·19	0·17
Al_2O_3	3·94	3·51	3·95	2·96	3·02	2·14	4·02	3·58	4·25	3·52	4·51	2·64	5·87	4·24	4·27	4·66	4·68	5·88	5·96	5·08	4·89	5·41	5·47
Cr_2O_3	0·46	0·35	0·45	0·29	0·25	0·20	0·31	0·25	0·44	0·27	0·59	0·23	0·47	0·60	0·60	0·73	0·73	0·43	0·41	0·36	0·36	0·58	0·55
FeO*	6·05	6·23	6·10	6·22	6·25	5·96	6·46	6·35	5·86	5·91	5·85	5·89	6·53	5·97	6·27	5·97	5·76	6·82	6·66	6·46	6·31	6·42	6·52
MnO	0·14	0·13	0·11	0·16	0·10	0·13	0·15	0·17	0·13	0·11	0·09	0·11	0·09	0·13	0·13	0·07	0·07	0·07	0·07	0·09	0·09	0·14	0·14
NiO	0·07	0·08	0·08	0·08	0·08	0·08	0·02	0·06	0·10	0·08	0·06	0·12	0·13	0·07	0·07	0·15	0·15	0·06	0·06	0·10	0·10	0·10	0·10
MgO	32·92	33·36	33·62	34·49	34·51	34·90	33·17	33·28	33·43	33·69	32·90	34·34	31·62	32·81	33·06	32·89	32·50	31·37	31·39	32·47	32·56	32·64	31·99
CaO	0·54	0·48	0·59	0·37	0·37	0·24	0·47	0·43	0·53	0·51	0·79	0·39	1·07	1·00	0·96	1·03	1·13	1·03	1·12	0·79	0·75	1·03	1·07
Na_2O	0·08	0·07	0·06	0·02	0·03	0·03	0·10	0·09	0·06	0·05	0·12	0·07	0·19	0·04	0·03	0·13	0·10	0·21	0·21	0·13	0·13	0·19	0·19
Total	99·16	99·62	100·11	100·28	100·48	100·03	100·17	100·18	99·46	100·08	100·00	100·33	99·65	99·18	100·15	100·69	99·43	99·74	99·86	100·30	100·22	100·05	99·56
Mg#	0·907	0·905	0·908	0·908	0·908	0·912	0·902	0·903	0·910	0·910	0·909	0·912	0·896	0·907	0·904	0·907	0·910	0·892	0·894	0·900	0·902	0·899	0·897

FeO* as total Fe; P and N designate porphyroclast and neoblast, respectively.

Table 2c: Representative microprobe analyses of clinopyroxenes from peridotite xenoliths from Nushan

	Amphibole-bearing peridotites											Ph-lherz	Amphibole-free peridotites							
Sample:	N-11	N-22		N-24		N-26		N-32		N-37		N-6	N-10		N-21	N-28		N-34		N-35
	core	core	rim	core	rim	core	rim	core	rim	core	rim		core	rim		core	rim	core	rim	
SiO_2	51·72	52·64	53·44	51·95	52·11	52·49	52·09	52·35	52·19	52·50	52·92	51·21	52·39	51·62	51·20	51·38	51·26	51·42	51·48	51·33
TiO_2	0·38	0·23	0·13	0·50	0·47	0·39	0·38	0·45	0·40	0·41	0·27	0·63	0·11	0·11	0·15	0·61	0·62	0·50	0·48	0·56
Al_2O_3	5·95	7·05	6·87	6·47	5·46	6·57	6·10	5·83	5·49	5·32	4·70	7·63	4·26	4·20	5·56	7·73	7·85	7·78	7·72	7·27
Cr_2O_3	1·17	1·11	1·25	1·07	0·84	0·76	0·67	0·94	0·75	0·93	1·09	0·82	0·75	0·74	1·15	0·70	0·70	0·87	0·85	0·99
FeO*	2·56	2·81	2·65	2·40	2·23	2·35	2·47	2·35	2·36	2·07	2·00	3·42	3·01	2·97	2·96	3·58	3·55	2·98	2·93	3·48
MnO	0·13	0·06	0·06	0·08	0·09	0·13	0·04	0·04	0·04	0·09	0·08	0·15	0·04	0·04	0·10	0·10	0·10	0·07	0·07	0·07
NiO	0·07	0·07	0·00	0·01	0·04	0·00	0·00	0·06	0·08	0·00	0·02	0·06	0·02	0·02	0·07	0·06	0·06	0·04	0·04	0·08
MgO	14·72	13·99	14·47	14·54	15·01	14·46	14·45	15·12	15·18	15·00	15·34	15·59	17·35	17·10	16·76	15·48	15·30	14·66	14·60	15·63
CaO	20·49	18·77	18·89	21·05	21·31	20·34	20·23	20·69	20·91	21·45	20·05	18·22	21·80	21·48	19·42	17·89	17·96	19·14	19·21	18·02
Na_2O	1·75	2·63	2·62	1·79	1·62	2·06	2·09	1·67	1·57	1·62	2·81	1·75	0·32	0·32	1·13	1·78	1·77	1·98	1·94	1·83
Total	98·93	99·40	100·37	99·90	99·21	99·57	98·51	99·51	98·96	99·41	98·79	99·50	100·10	98·30	98·50	99·32	99·16	99·45	99·32	99·27
Mg#	0·911	0·899	0·907	0·915	0·924	0·917	0·912	0·920	0·920	0·928	0·932	0·890	0·912	0·910	0·910	0·885	0·886	0·897	0·897	0·889

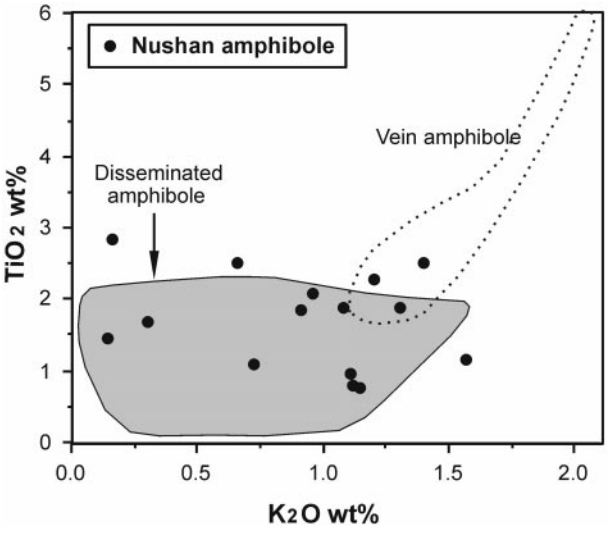

Fig. 2. Comparison of TiO_2 and K_2O contents in amphiboles in Nushan peridotites with interstitial and vein amphiboles from other xenolith localities (Francis, 1976; Witt & Seck, 1989; Ionov & Hoffmann, 1995; Vaselli *et al*., 1995; Chazot *et al*., 1996).

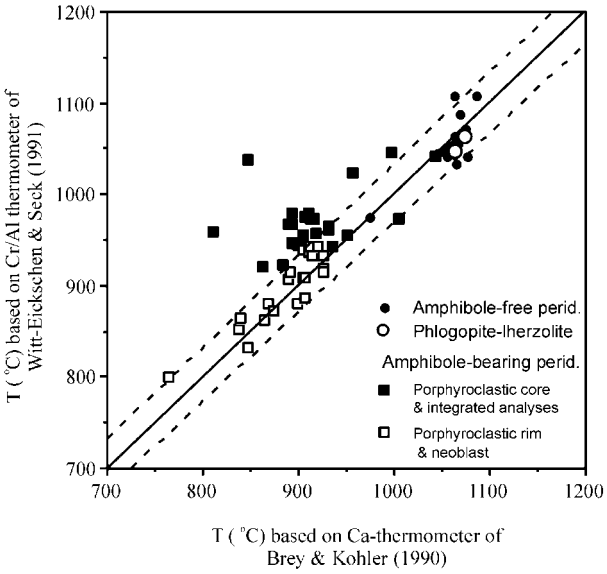

Fig. 3. Comparison of the temperature estimates for the Nushan peridotite xenoliths based on the Ca-orthopyroxene thermometer of Brey & Kohler (1990) and on the Cr/Al-orthopyroxene thermometer of Witt-Eickschen & Seck (1991). The domain between the two dashed lines is for ideal correlation ±25°C. Points for porphyroclastic rims and neoblasts are more than the number of the analysed samples, because multiple analyses have been performed on core–rim and neoblasts for each sample.

(Wilkinson & Le Maitre, 1987). With respect to Ti, the Nushan amphiboles are intermediate between low-Ti amphiboles (Francis, 1976; Witt & Seck, 1989; Ionov & Hoffmann, 1995; Chazot *et al*., 1996) and high-Ti amphiboles found in black pyroxenite veins and wall-rock peridotites (Witt & Seck, 1989; Ionov & Hoffmann, 1995; Vaselli *et al*., 1995) (Fig. 2). Amphibole Mg# values range from 0·883 to 0·904, similar to the Mg# range in coexisting silicate minerals.

Pyroxenes are compositionally homogeneous in amphibole-free peridotites (Table 2b and c). In contrast, orthopyroxenes in amphibole-peridotites are generally zoned regardless of the textural type, with contents of Al and Cr decreasing from cores to rims, whereas Si and Mg show the opposite trend (Table 2b). In half of the amphibole-peridotites examined, the contents of Ca in opx decrease toward the rims. Small neoblasts are compositionally similar to porphyroclast rims. The amphibole-peridotites are further distinguished from the amphibole-free samples by lower contents of Al, Cr and Ca in opx (Table 2b). Al in cpx decreases from core to rim. However, Cr in cpx either slightly decreases (N-24, N-26, N-32) or slightly increases (N-22, N-37) (Table 2c).

Temperature estimates

Mineral chemistry indicates that chemical equilibrium between minerals was almost attained in the amphibole-free samples, whereas the amphibole-peridotites show conspicuous evidence for inter-mineral disequilibrium. Thus, the temperature estimates for the amphibole-peridotites were performed independently for porphyroclasts and neoblasts, as well as for cores and rims. The temperatures were calculated with the two-pyroxene and the Ca-in-opx thermometers of Brey & Kohler (1990), as well as with the empirical thermometer of Witt-Eickschen & Seck (1991), based on Cr–Al exchange between opx and spinel. For the amphibole-free peridotites, there is a good agreement between the temperatures (990–1110°C) calculated with the three thermometers (Table 1; Fig. 3). The equilibrium temperatures of two phlogopite-bearing peridotites are ~1100°C, thus comparable with that of the amphibole-free samples (Table 1).

For the porphyroclast cores in amphibole-peridotites, the Al–Cr-opx thermometer provides higher temperature estimates than the Ca-in-opx thermometer (Table 1; Fig. 3). Temperatures as high as 1047°C were obtained for integrated analyses on unmixed opx porphyroclasts. In contrast, the temperatures (850–950°C) estimated by these two thermometers for porphyroclast rims and neoblasts are essentially the same (within ±25°C; Fig. 3), and are significantly lower than those for amphibole-free samples. For the opx exhibiting homogeneity relative to Ca, the Ca-in-opx thermometer gives similar estimates for both the core and rim compositions (e.g. N-22, N-26, N-32). Such a phenomenon is often observed for disequilibrium spinel lherzolites (Preß *et al*., 1986; Witt &

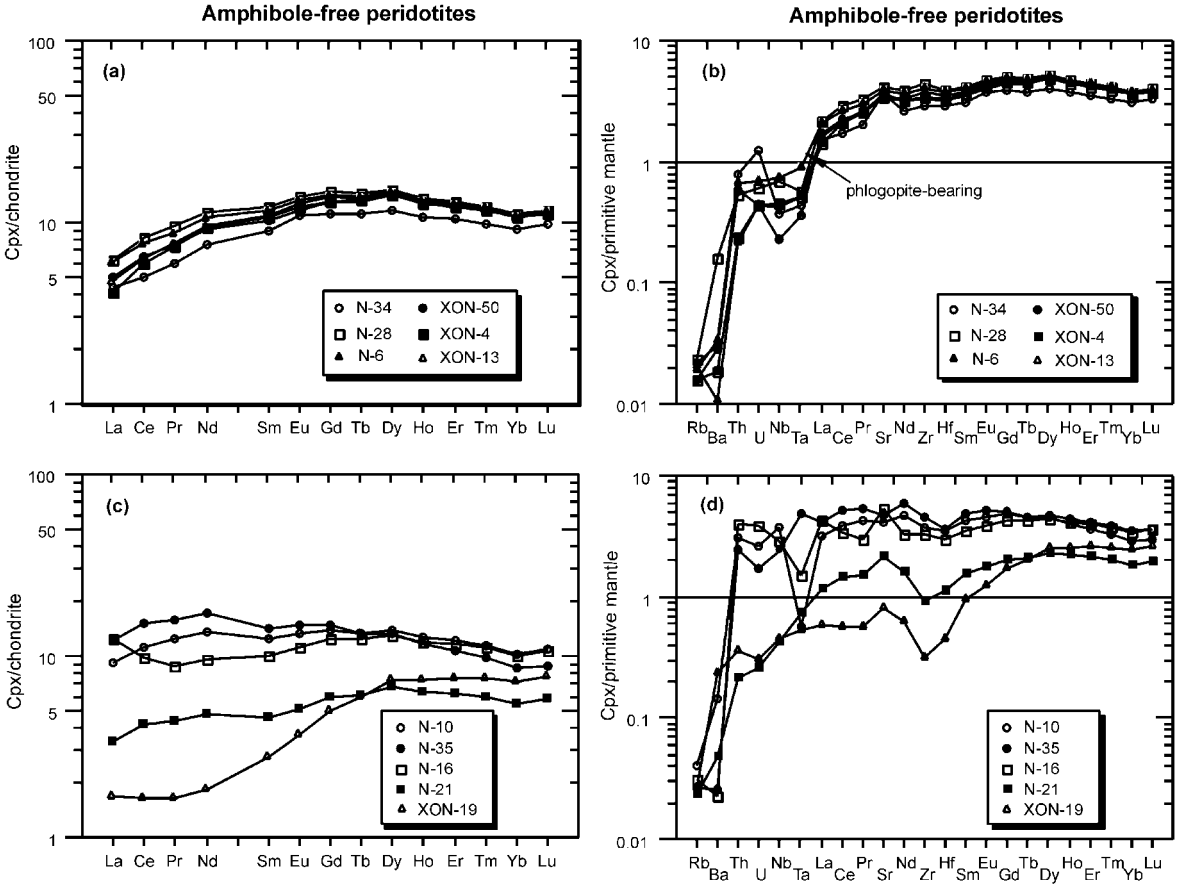

Fig. 4. REE and trace element abundances in clinopyroxenes from the anhydrous peridotites and from phlogopite peridotites (N-6, XON-13) from Nushan. Normalizing data after Sun & McDonough (1989).

Seck, 1987; Xu *et al.*, 1993; Werling & Altherr, 1997) and can be accounted for by higher diffusion velocity of Ca in pyroxenes relative to that of Al (Sautter *et al.*, 1988) during the changing physical conditions. It is inferred that the Nushan amphibole-peridotites record a cooling history from about 1050°C to 850°C. This cooling event is consistent with the presence of exsolution lamellae in opx in the amphibole-bearing suite. It is clear that application of the two-pyroxene thermometer to the amphibole-bearing peridotites is problematic, because true equilibrium between pyroxenes cannot be demonstrated. However, the general absence of cpx porphyroclasts in these rocks permits us to assume that the mineral pairs of cpx and opx rim or neoblasts would yield the latest equilibrium temperature. The temperatures estimated by the two-pyroxene thermometer of Brey & Kohler (1990) are virtually consistent with those based on single thermometers (Table 1), supporting this assumption. It is thus concluded that amphibole-bearing peridotites equilibrated at a lower temperature (850–950°C) than amphibole-free ones (990–1110°C).

Trace element composition

Clinopyroxene in amphibole-free peridotites

Two types of trace element patterns have been recognized in cpx from amphibole-free samples. The first is characterized by relatively high heavy REE (HREE) contents (Yb_n = 9·1–11·1, n = chondrite-normalized value) and light REE (LREE)-depleted chondrite-normalized REE patterns with $(La/Yb)_n$ varying between 0·45 and 0·56 (Fig. 4a). These cpx are strongly depleted in Rb and Ba. All cpx from this group show small to significant negative anomalies of Nb and Ta (Fig. 4b). Cpx from phlogopite-bearing peridotites are comparable with the depleted cpx in amphibole-free samples with respect to their trace element signature, except for having less significant Nb–Ta negative anomalies (Fig. 4b).

The second group of cpx is distinguished by lower HREE contents (Yb_n = 5·4–10·3; Fig. 4c). They are either slightly enriched in LREE and middle REE (MREE) relative to HREE, with convex-upward chondrite-normalized REE patterns (N-10, N-35), or enriched in LREE relative to MREE, with 'spoon-shaped'

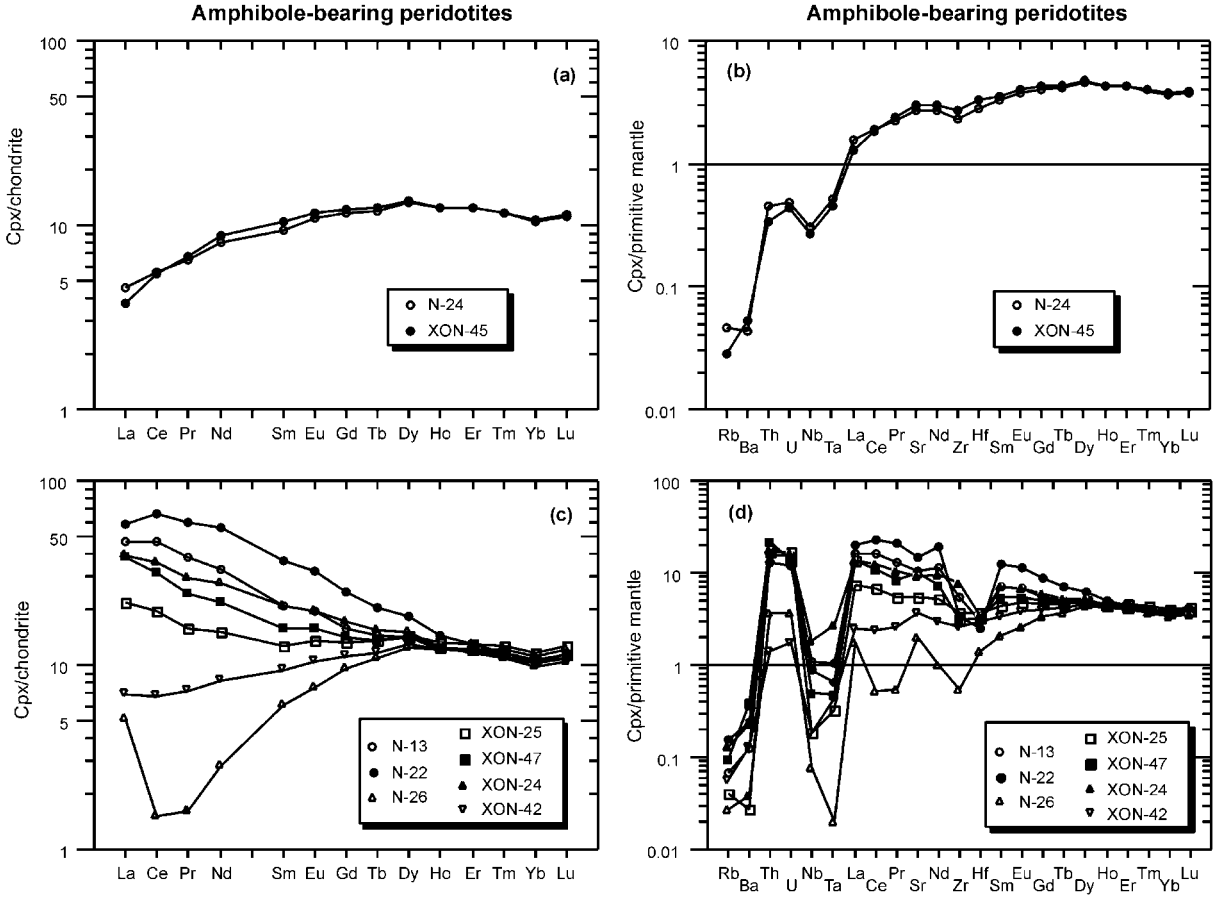

Fig. 5. REE and trace element abundances in clinopyroxenes from amphibole-bearing peridotites from Nushan. Normalizing data after Sun & McDonough (1989).

REE patterns (N-16, XON-19). Cpx of sample N-21 is depleted in LREE relative to MREE but otherwise displays several features typical of the latter group. In this group, the cpx with the lowest Yb_n (5·4–7·2) are depleted in Th, U, Nb and Ta relative to LREE on the primitive mantle (PM)-normalized diagrams and show a negative Zr–Hf anomaly. The other cpx show a relatively flat distribution from Th to Lu (Fig. 4d) with negative or positive anomalies for Ta but not for Nb.

Clinopyroxene in amphibole-bearing peridotites

Cpx in amphibole-bearing samples have a wide range of LREE concentrations (Ce_n = 1·7–70) compared with the restricted HREE variation (Yb_n = 9·8–11·6) (Fig. 5a and c). Two samples (N-24, XON-45), in which only rare amphibole grains are observed, display cpx REE patterns very similar to those of the LREE-depleted cpx in the amphibole-free suite, except for a slight negative Zr anomaly (Fig. 5a and b). However, most cpx from amphibole-peridotites are enriched in LREE. Sample N-26 with a tabular equigranular texture shows the lowest Ce content. The degree of LREE enrichment in cpx is broadly correlated with the abundance of amphibole in the samples. Peridotites that contain 3·5–5% amphibole (e.g. N-22, N-13) show LREE concentrations >10 × chondrite whereas those that contain <1% amphibole have lower LREE contents. Except for the two LREE-depleted samples, cpx of the amphibole-bearing peridotites have PM-normalized contents of Th and U at about the same level as LREE. In contrast, Nb and Ta are strongly depleted relative to these elements, whereas Zr and/or Hf tend to show negative anomalies relative to MREE. Rb and Ba concentrations are higher than in the other analysed cpx.

Whole rocks

Three whole-rock analyses are listed in Table 3 and are compared with cpx composition in Fig. 6a and b. For a given sample, whole rock and cpx generally display similar REE patterns except that the concentration

Table 3: Trace element composition (ppm) and Sr-Nd isotopes in clinopyroxenes from Nushan peridotite xenoliths

	Amphibole-free peridotites												Phl. perid.		Amphibole-bearing peridotites								
Sample:	N-10	N-35	N-16	N-21	N-28	N-34	XON-4	XON-4*	XON-19	XON-19*	XON-50	XON-50*	N-6	XON-13	N-13	N-22	XON-25	XON-47	XON-24	N-26	XON-42	N-24	XON-45
Rb	0·03	0·02	0·02	0·02	0·02	0·01	0·01	0·05	0·02	0·11	0·01	0·06	0·01	0·01	0·04	0·10	0·03	0·06	0·08	0·02	0·03	0·03	0·02
Sr	86·6	99·5	113·2	45·5	87·8	76·1	71·9	12·2	17·4	5·56	76·5	38·9	82·8	72·2	217·3	315·7	115·9	214·2	192·4	42·6	74·6	57·5	64·0
Y	16·08	14·58	15·58	8·19	17·43	13·82	16·25	2·88	9·58	1·38	16·47	2·59	16·93	16·61	16·19	19·38	17·62	16·89	16·29	15·87	15·69	16·31	16·19
Zr	41·51	51·28	36·57	10·48	49·42	32·96	38·73	7·50	3·59	1·18	37·19	6·23	44·38	41·76	59·94	37·65	41·47	35·27	84·86	6·22	27·51	26·20	30·56
Nb	2·64	1·69	2·06	0·30	0·49	0·27	0·32	0·27	0·32	0·46	0·17	0·58	0·52	0·30	0·79	0·61	0·13	0·35	1·33	0·05	0·12	0·22	0·19
Ba	1·03	0·18	0·16	0·33	1·12	0·21	0·13	2·43	1·66	1·46	0·20	14·82	0·23	0·08	0·88	1·66	0·19	2·67	1·60	0·26	0·89	0·30	0·36
La	2·17	2·86	2·94	0·81	1·48	1·03	0·97	0·36	0·40	0·24	1·19	1·29	1·43	1·12	11·01	13·90	5·13	9·19	9·24	1·21	1·64	1·08	0·89
Ce	6·85	9·18	6·02	2·56	5·07	3·08	3·67	0·60	1·00	0·36	3·96	2·38	4·74	3·88	28·56	40·24	11·93	19·37	21·96	0·93	4·13	3·39	3·30
Pr	1·19	1·50	0·83	0·41	0·91	0·57	0·70	0·13	0·16	0·05	0·71	0·28	0·83	0·73	3·65	5·69	1·51	2·32	2·84	0·15	0·68	0·62	0·65
Nd	6·39	7·98	4·44	2·22	5·32	3·53	4·33	0·73	0·86	0·23	4·30	1·22	4·93	4·45	15·50	26·21	6·99	10·15	13·04	1·34	3·88	3·72	4·06
Sm	1·89	2·19	1·54	0·70	1·87	1·38	1·62	0·26	0·42	0·08	1·57	0·33	1·77	1·69	3·20	5·61	1·96	2·40	3·17	0·94	1·43	1·45	1·59
Eu	0·77	0·86	0·65	0·30	0·80	0·63	0·70	0·11	0·21	0·03	0·68	0·13	0·77	0·73	1·14	1·89	0·79	0·93	1·15	0·44	0·61	0·63	0·67
Gd	2·87	3·03	2·54	1·22	3·01	2·30	2·69	0·44	1·03	0·16	2·66	0·47	2·92	2·85	3·26	5·18	2·76	2·91	3·52	1·97	2·31	2·38	2·53
Tb	0·49	0·49	0·46	0·23	0·53	0·41	0·49	0·08	0·22	0·03	0·48	0·08	0·52	0·50	0·53	0·75	0·50	0·51	0·57	0·40	0·43	0·44	0·46
Dy	3·54	3·38	3·30	1·71	3·82	2·99	3·56	0·59	1·86	0·26	3·57	0·54	3·75	3·66	3·63	4·63	3·69	3·60	3·80	3·17	3·27	3·38	3·43
Ho	0·72	0·66	0·68	0·36	0·78	0·62	0·73	0·13	0·42	0·06	0·74	0·11	0·76	0·75	0·70	0·82	0·76	0·72	0·71	0·69	0·69	0·71	0·71
Er	2·00	1·77	1·91	1·03	2·14	1·72	2·02	0·37	1·26	0·19	2·09	0·33	2·11	2·08	1·96	2·14	2·17	2·03	1·95	2·03	1·98	2·04	2·05
Tm	0·29	0·25	0·28	0·15	0·31	0·25	0·29	0·06	0·19	0·03	0·30	0·05	0·30	0·30	0·28	0·29	0·32	0·29	0·27	0·30	0·29	0·29	0·29
Yb	1·75	1·45	1·70	0·92	1·88	1·54	1·82	0·37	1·22	0·20	1·85	0·32	1·85	1·80	1·73	1·77	1·97	1·82	1·67	1·89	1·80	1·83	1·79
Lu	0·27	0·22	0·27	0·15	0·29	0·24	0·28	0·06	0·19	0·04	0·29	0·05	0·29	0·28	0·27	0·27	0·32	0·29	0·26	0·30	0·28	0·29	0·28
Hf	1·08	1·14	0·93	0·35	1·20	0·89	1·01	0·18	0·14	0·03	0·99	0·16	1·15	1·09	0·91	0·78	1·14	1·01	1·05	0·43	0·87	0·88	1·03
Ta	0·02	0·20	0·06	0·03	0·02	0·02	0·02	0·01	0·02	0·02	0·01	0·01	0·04	0·02	0·04	0·03	0·01	0·02	0·11	0·00	0·02	0·02	0·02
Pb	0·13	0·08	0·06	0·06	0·09	0·06	0·05	0·15	0·07	0·15	0·10	0·26	0·06	0·04	0·43	0·49	0·33	0·45	0·36	0·22	0·20	0·18	0·08
U	0·06	0·04	0·09	0·01	0·01	0·03	0·01	0·00	0·01	0·01	0·01	0·03	0·02	0·01	0·36	0·27	0·39	0·31	0·37	0·09	0·04	0·01	0·01
Th	0·26	0·21	0·34	0·02	0·05	0·07	0·02	0·01	0·03	0·03	0·05	0·19	0·06	0·02	1·30	1·11	1·45	1·88	1·48	0·31	0·11	0·04	0·03
$^{87}Sr/^{86}Sr$		0·703410			0·703576								0·702613			0·703284			0·703088				
2 SD		0·000010			0·000010								0·000011			0·000010			0·000010				
$^{143}Nd/^{144}Nd$		0·512840			0·512901								0·513213			0·512942			0·512986				
2 SD		0·000004			0·000005								0·000004			0·000005			0·000004				

*Whole-rock analyses.

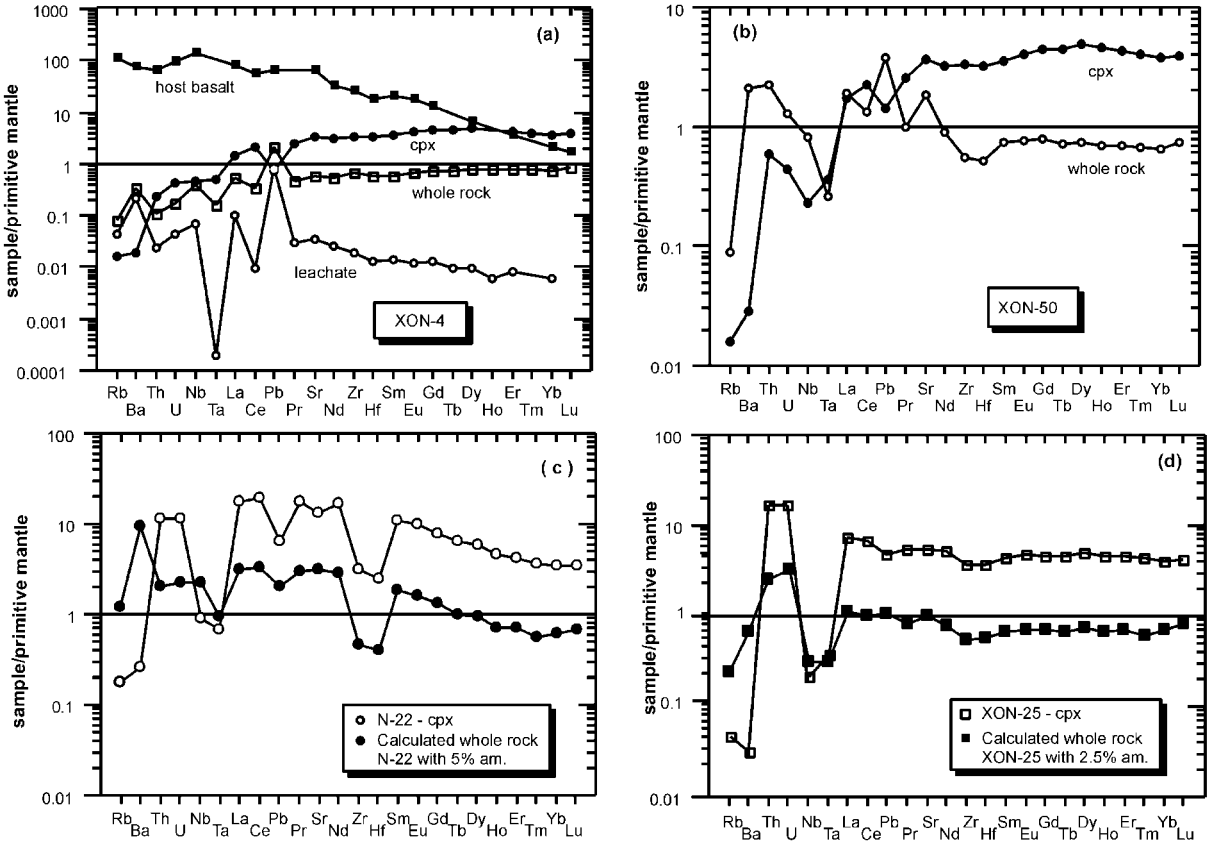

Fig. 6. Comparison between trace element compositions in clinopyroxenes and whole rocks. (a, b) Amphibole-free samples; (c, d) amphibole-bearing peridotites. The whole-rock compositions of amphibole-bearing peridotites are calculated using the compositions of cpx, modal composition and the partition coefficients of Ionov & Hoffmann (1995) and Eggins *et al.* (1998). The host basalt data are from Liu *et al.* (1994).

level is higher for cpx. However, the concentrations of Rb, Ba, Th, U and Pb in whole rocks tend to be higher than those in cpx (Fig. 6a and b), probably as a result of intergranular materials that are rich in highly incompatible elements. This is supported by analyses of HCl leachates of cpx separates, which are characterized by steadily enriched patterns with positive Sr and Pb, and negative Nb, Zr and Hf anomalies (Fig. 6a).

Sr–Nd isotopes in clinopyroxene separates

Cpx from two amphibole-peridotites have $^{87}Sr/^{86}Sr$ = 0·7031–0·7033 and $^{143}Nd/^{144}Nd$ = 0·51294–0·5130 (Table 3). Similar isotopic compositions are found for cpx from two amphibole-free samples ($^{87}Sr/^{86}Sr$ = 0·7034–0·7036 and $^{143}Nd/^{144}Nd$ = 0·5128–0·5129). One phlogopite-bearing sample (N-6) has slightly lower $^{87}Sr/^{86}Sr$ (0·7026) and higher $^{143}Nd/^{144}Nd$ (0·5132). Despite the limited number of analyses, these isotopic values are similar to those defined by eight whole-rock analyses reported by Xu *et al.* (1998*a*). The amphibole-bearing samples and Fe-rich amphibole-free peridotites plot within the field of the Cenozoic basalts from eastern China and isotopically resemble the host basalts (Fig. 7).

DISCUSSION

Comparison between whole-rock and cpx data

In this study, ICP-MS analyses were mainly performed on cpx separates. The choice of cpx rather than bulk rock is largely because most of the Nushan xenoliths are not sufficiently fresh as a result of surface alteration and also because large amounts of trace elements reside in cpx. Analysed whole rocks generally have higher ratios of highly incompatible elements (HIE) to HREE compared with cpx (Table 3; Fig. 6a and b). This feature is mainly related to the presence of fluid inclusions in ol and opx, and subordinately to interstitial components (Bedini & Bodinier, 1999). The same inclusions generally exist in cpx but have less of an effect on the HIE/HREE ratios because of the higher HIE content in cpx. Given the difficulties in quantifying the contribution of fluid inclusion and intergranular components to the budget of trace elements in the whole rocks, and

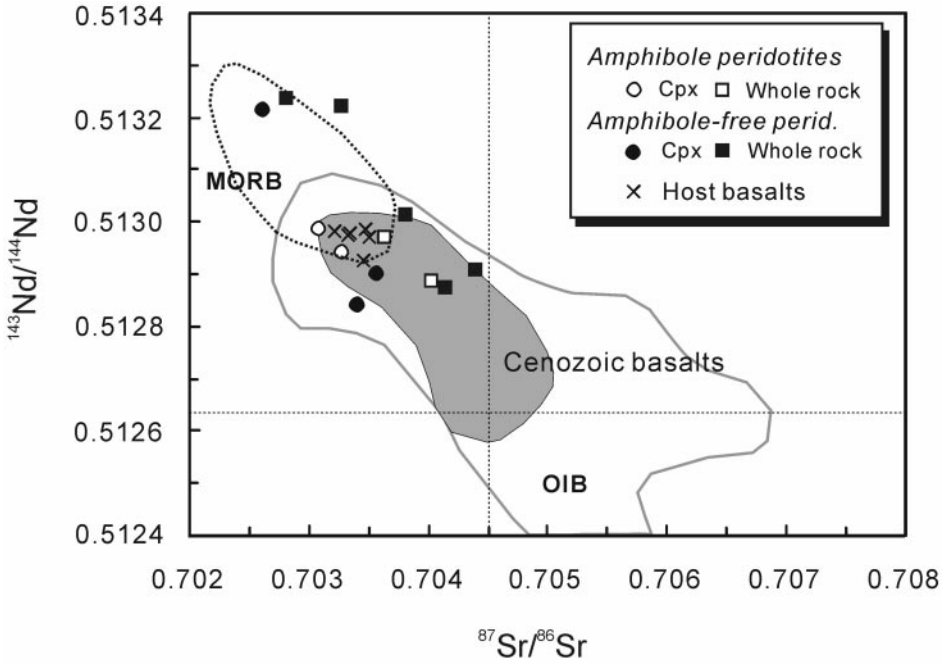

Fig. 7. $^{143}Nd/^{144}Nd$ vs $^{87}Sr/^{86}Sr$ for clinopyroxene separates and whole rocks (Xu *et al*., 1998*a*) from the Nushan peridotites. Isotope data for Cenozoic alkaline basalts (Peng *et al*., 1986; Song *et al*., 1990; Basu *et al*., 1991; Zou *et al*., 2000) from eastern China are given for comparison. Mid-ocean ridge basalt (MORB) and ocean island basalt (OIB) domains are after Zindler & Hart (1986).

the controversy over the origin of intergranular components, cpx may provide more decipherable and straightforward information on mantle processes than whole rocks (except for hydrous peridotites) (Bedini & Bodinier, 1999).

Even for the amphibole-bearing peridotites, the REE pattern in cpx can still be considered representative of the whole-rock pattern, because cpx and amphibole have very similar partition coefficients for REE (Ionov & Hoffman, 1995; Tiepolo *et al*., 2001; Ionov *et al*., 2002). However, this is not the case for Nb and Ta because these elements are preferentially partitioned into amphibole (Ionov & Hoffmann, 1995; Tiepolo *et al*., 2001) and Ti-oxides (Bodinier *et al*., 1996; Kalfoun *et al*., 2002), relative to cpx. This effect can be evaluated by reconstructing the whole-rock compositions, using the compositions of cpx, modal composition and partition coefficients of Ionov & Hoffmann (1995) and Eggins *et al*. (1998). As shown in Fig. 6c, Nb depletion in whole rocks with relatively abundant amphibole (~5%) is significantly smaller than in cpx, as a result of the counterbalance of amphibole. In samples with less amphibole (<3%), the trace element composition in the whole rock is predominantly controlled by cpx (Fig. 6d). As most samples from Nushan contain <1% amphibole, it can be concluded that the distinct geochemical features shown by cpx (Figs 4 and 5) are largely related to open-system mantle processes, rather than subsolidus partitioning.

Definition: 'diffuse' and 'wall-rock' metasomatism

Two different mechanisms of metasomatism have been proposed to explain the geochemical characteristics of peridotites. Both are related to melt transport in the mantle. 'Wall-rock' metasomatism is related to melt transport in fractures forming veins and dykes and is regarded as a local phenomenon. Compositional and textural changes caused by interaction with melts from the fracture are generally confined to the wall-rocks (Kempton, 1987). In this model, modally metasomatized peridotites generally occur adjacent to vein conduits, whereas cryptically metasomatized peridotites are more distant (Menzies *et al*., 1985). The wall-rock peridotites adjacent to veins are generally characterized by convex-upward or flat REE patterns and Fe enrichment.

'Diffuse' metasomatism corresponds to melt migration by percolation along grain boundaries in a solid matrix (i.e. porous flow). In this model, the reactional surface is nearly unlimited; therefore the infiltrated melt is likely to interact more strongly (Navon & Stolper, 1987). The metasomatic agent involved is generally a small melt fraction rich in volatiles. Such melts are believed to have low viscosities and solidification temperatures and are able to pervasively infiltrate large volumes of relatively cold lithospheric peridotites (McKenzie, 1989; Kelemen *et al*., 1995; Bedini *et al*., 1997; Xu *et al*., 1998*c*). Diffuse metasomatism is

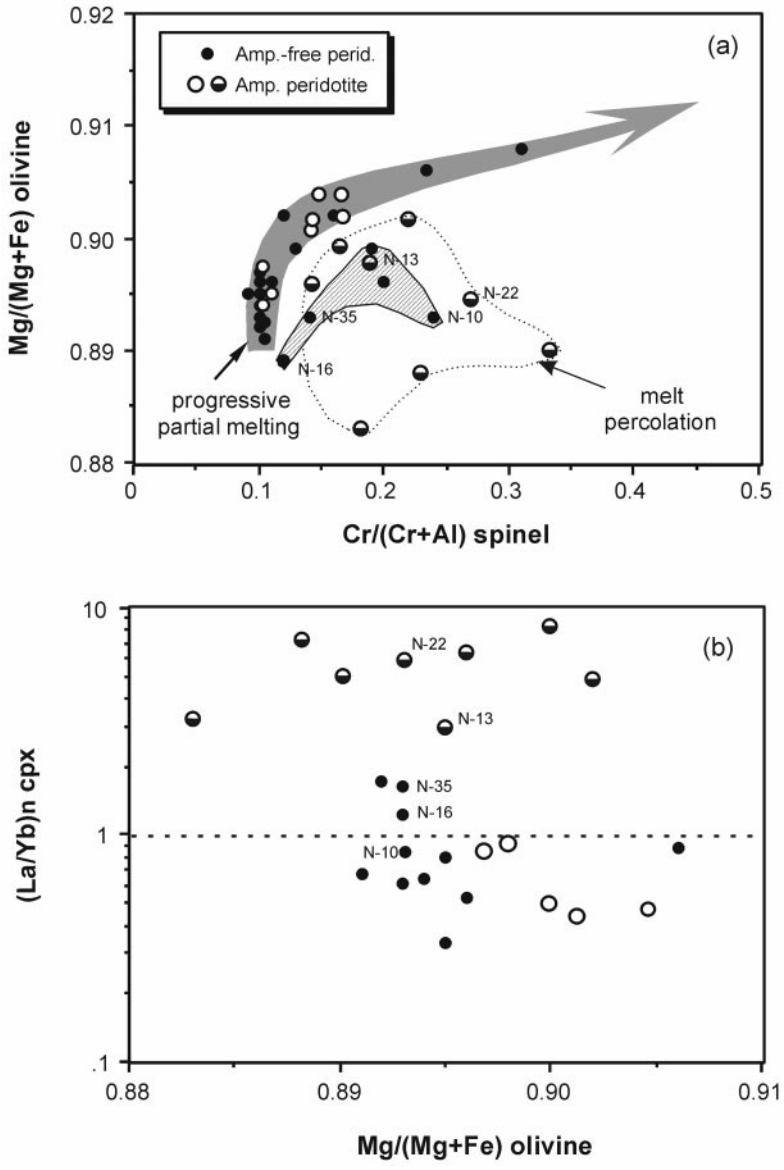

Fig. 8. (a) Correlation of Cr/(Cr + Al) of spinel ($Cr\#_{sp}$) vs Mg/(Mg + Fe) of olivine ($Mg\#_{ol}$). The progressive partial melting trend is from Xu *et al.* (1998*c*); (b) La/Yb of clinopyroxene vs $Mg\#_{ol}$. Data from Xu *et al.* (1998*a*) are also included.

generally characterized by a lack of Fe enrichment and highly fractionated REE patterns ranging from U-shaped to steadily enriched patterns (Bodinier *et al.*, 1990; Bedini *et al.*, 1997; Ionov *et al.*, 2002). It is now widely accepted that chromatographic processes, such as proposed by Navon & Stolper (1987), can account for the selective enrichment of incompatible elements in many peridotites.

Amphibole-free peridotites: 'wall-rock' metasomatism

To define the mechanism of metasomatism that has been active within the mantle beneath Nushan, it is important to evaluate whether the samples in question are Fe-rich or not. The co-variation diagram of $Mg\#_{ol}$ vs $Cr\#_{sp}$ can be used for this purpose (Fig. 8a). It has been shown by studies on natural samples (Cabanes & Mercier, 1988) and by experiments (Jaques & Green, 1980) that incipient partial melting is characterized by a progressively increasing $Mg\#_{ol}$ and nearly constant $Cr\#_{sp}$, whereas more intense partial melting gives rise to a significant increase in $Cr\#_{sp}$ and only a slight increase in $Mg\#_{ol}$. Samples that plot below this progressive partial melting trend are generally ascribed to Fe enrichment (e.g. Xu *et al.*, 1998*c*). Some amphibole-free peridotites from Nushan are characterized by

relatively low $Mg\#_{ol}$ at given $Cr\#_{sp}$, compared with the partial melting trend (Fig. 8a). It is these Fe-rich samples that show LREE enrichment (Fig. 8b). The coexistence of Fe-rich, LREE-enriched peridotites and 'normal' LREE-depleted ones agrees with the view that the amphibole-free lherzolites represent mantle fragments adjacent to basic dykes (Menzies *et al.*, 1985). Usually, peridotites affected by wall-rock metasomatism are only mildly enriched in LREE as they have equilibrated with liquids of broadly basaltic composition. Cpx in such peridotites tend to show upward convex REE patterns, slight LREE enrichment and are devoid of negative HFSE anomalies or show only subtle ones (Menzies *et al.*, 1985; Bodinier *et al.*, 1990). These features predicted by 'wall-rock' metasomatism are essentially found in the Nushan amphibole-free samples (Fig. 4). Using crystal/melt partition coefficients (Hart & Dunn, 1993; Hauri *et al.*, 1994), the REE concentrations in cpx can be used to estimate the trace element composition of melts in equilibrium with cpx from the Fe-rich peridotites, if the assumption of equilibrium between cpx and melt is valid. The compositional similarity between the hypothesized equilibrium melts and the host basalts (Fig. 9a) thus lends further support to the 'wall-rock' metasomatism model. As discussed above, Fe enrichment is generally confined to wall-rocks within a few centimetres of veins (e.g. Kempton, 1987; Bodinier *et al.*, 1990). The variation of trace element patterns in the amphibole-free samples is therefore probably related to the distance from basaltic veins (Fig. 10b).

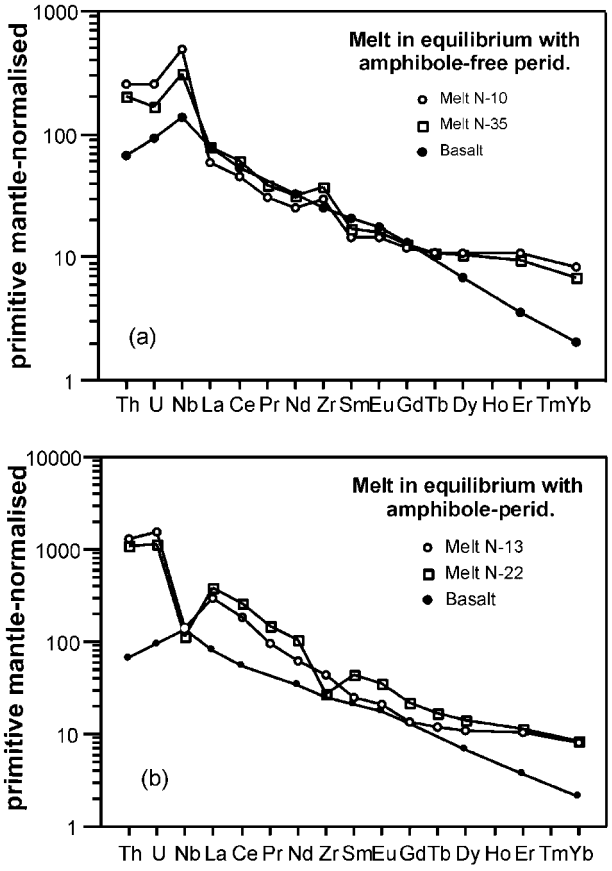

Fig. 9. Calculated trace element abundances in melts in equilibrium with the amphibole-free peridotites (a) and amphibole-bearing peridotites (b). Partition coefficients between cpx and melt are from Hart & Dunn (1993) and Hauri *et al.* (1994). Data for the host basalts are from Liu *et al.* (1994).

Amphibole-bearing peridotites: 'diffuse' and 'wall-rock' metasomatism

The amphibole-peridotites from Nushan have distinctly lower temperature estimates than the amphibole-free ones (Table 1; Fig. 3). The higher temperature of the amphibole-free samples may be due to heating associated with the dykes. However, as discussed below, the Fe-rich amphibole-bearing peridotites may also have been close to the dykes, but they have a much lower temperature. Transient heating would result in increase in Ca and Al contents from core to rim in opx (e.g. Witt-Eickschen & Seck, 1991). This is not the case at Nushan. Alternatively, the equilibrium temperatures measured in the xenoliths may represent the *in situ* temperature at the time of entrainment and the xenoliths were equilibrated on the same conductive geotherm (e.g. Zangana *et al.*, 1997). Thus, the amphibole-bearing and amphibole-free peridotites may represent, respectively, the shallower and deeper parts of the mantle lithosphere (Fig. 10a). In the shallower part, there are no amphibole-free peridotites (Table 1), suggesting that the amphibole-bearing lherzolites may represent pervasively metasomatized shallow mantle. The range of trace element patterns and pronounced HFSE negative anomalies in cpx in amphibole-peridotites are also consistent with 'diffuse' metasomatism. As shown by Vernières *et al.* (1997) and Bedini *et al.* (1997), such a large range of LREE variations associated with almost constant HREE can be explained by reactive porous flow metasomatism by small melt fractions. Similar results have been obtained by recent trace element modelling for the amphibole-free and amphibole-bearing peridotite xenoliths from Spitsbergen (Ionov *et al.*, 2002).

However, the 'diffuse' metasomatism model is not consistent with the Fe enrichment in the amphibole-rich samples (Fig. 8a). A decrease in $Mg\#_{ol}$ from 0·90–0·91 to about 0·89 by metasomatism would require very high melt/rock ratios (Kelemen *et al.*, 1995), which can be achieved only in wall-rocks close to vein conduits or in magma channels. It is thus possible that both 'wall-rock' and 'diffuse' metasomatism

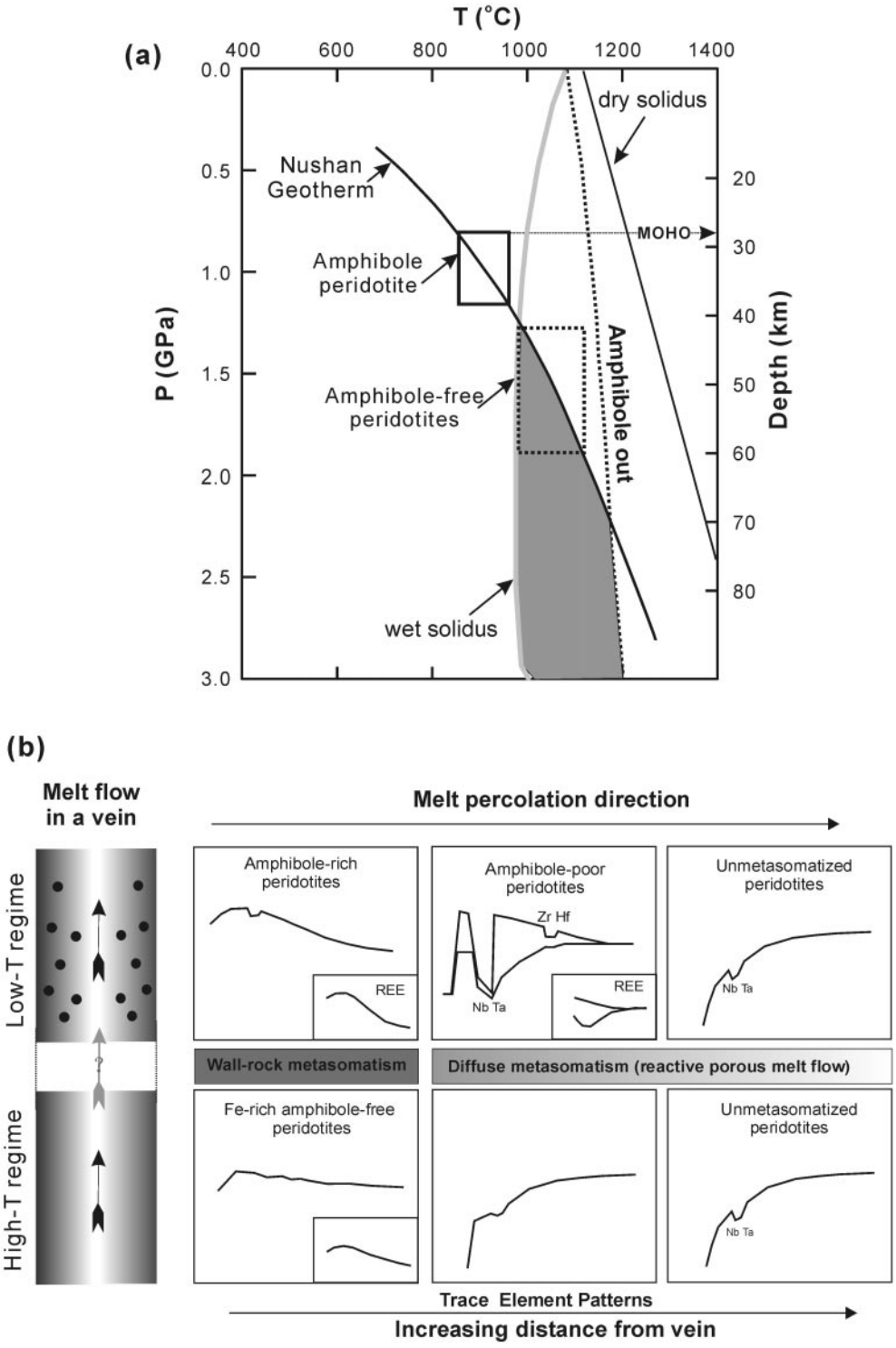

Fig. 10. (a) Interpretation of the thermometric data for the Nushan peridotite xenoliths in terms of depth–temperature context. The stability field of amphibole and the geotherm are from Wallace & Green (1991) and Xu *et al.* (1998*a*), respectively. The shaded area outlines the region of partial melting under hydrous conditions. (b) A scheme illustrating a possible genetic relationship between the amphibole-free and amphibole-bearing peridotites. The range of trace element patterns observed in the respective suites can be ascribed to melt percolation in the peridotites adjacent to veins or dykes. The melt flows in the low-temperature regime (amphibole-bearing domain), which are rich in volatiles and incompatible elements, are probably evolved derivatives from the asthenosphere-derived basaltic melts that precipitated early anhydrous assemblages in the high-temperature regime (amphibole-free domain). (See text for details.)

were involved in the formation of the amphibole-bearing samples. Different styles of metasomatism with distance to dykes have been previously observed in peridotite massifs (e.g. Bodinier *et al*., 1990) and ascribed to a single metasomatic event involving progressive chemical evolution of melt infiltrated in lithospheric peridotites and gradually solidifying down a thermal gradient.

LREE enrichment mainly occurs in the amphibole-peridotites that deviate from the partial melting trend (Fig. 8a and b). The highest HIE contents occur in the samples with the most abundant amphibole. This suggests that amphibole-rich peridotites (e.g. N-22, N-13) may have been close to the melt/dyke source and their compositions approach equilibrium with the percolating melts. The high contents of incompatible elements in these samples must reflect those of the percolating melts, which may be different from the counterpart involved in the amphibole-free peridotites (Fig. 9b). In contrast, amphibole-poor samples (e.g. N-24, N-26) may have been relatively far away from the dykes, in a region where a diffuse mechanism was operative (Fig. 10b). In addition to the metasomatic mechanism, progressive chemical change of the percolating melts also played an important role in generating a wide spectrum of trace element patterns in the amphibole-peridotites. It is likely that crystallization of amphibole in vein conduits and wall-rock peridotites resulted in a significant decrease in water and Nb–Ta contents in the residual melts. As a consequence, at greater distances from the dykes, the water-poor and Nb–Ta-deficient melts produced amphibole-poor peridotites, which are characterized by LREE–HFSE fractionated trace element signatures (Fig. 10b).

In a Sm–Hf diagram (Fig. 11), cpx in the amphibole-peridotites are different from those in high-Ti amphibole-peridotites and clinopyroxenites, which are closely related to vein system metasomatism (e.g. Witt-Eickschen *et al*., 1993). Nevertheless, the TiO_2 content of the Nushan amphiboles (Table 2a; Fig. 2) is relatively high compared with low-Ti amphiboles for which H_2O–CO_2 fluids have been invoked as metasomatic agents (Francis, 1976; Witt & Seck, 1989). This suggests that H_2O and CO_2 fluids may not be the metasomatic agents in the Nushan case because Ti is relatively insoluble in H_2O and CO_2 fluids (Schneider & Eggler, 1986). The metasomatic agents involved in the amphibole-peridotites may be different from the host basalts, judging from the higher REE contents in calculated melts in equilibrium with amphibole-peridotites than the host basalts (Fig. 9b). The metasomatic agent could be either a carbonate melt (Ionov *et al*., 1993) or a volatile-rich silicate melt similar to that described by McKenzie (1989). As modelled by Bedini *et al*. (1997), small fractions of these melts saturated in Ti-oxides may become strongly LILE enriched and Nb–Ta depleted during migration through lithospheric mantle.

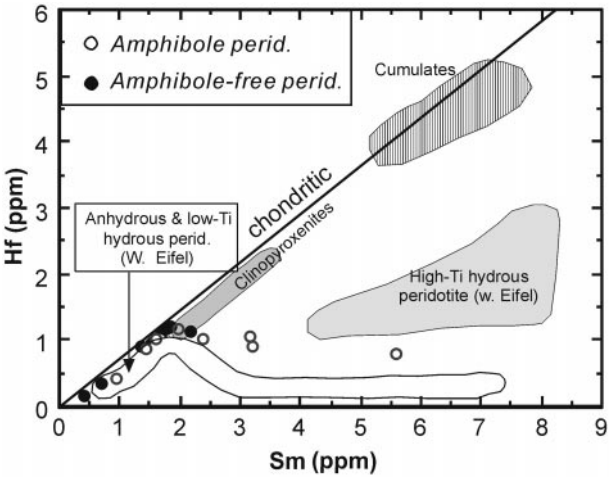

Fig. 11. Sm vs Hf in clinopyroxenes from the Nushan peridotites. Data for West Eifel are after Witt & Seck (1989) and Witt-Eickschen *et al*. (1993).

Multiple enrichments or a single event?

In summary, the Nushan xenoliths are likely to have been sampled from two different, spatially separated metasomatic aureole systems (Fig. 10). Amphibole-free peridotites are samples of mantle rocks adjacent to basaltic veins, whereas the melts/dykes responsible for formation of the amphibole-peridotites were rich in water and incompatible elements. At first sight, this appears to require two distinct metasomatic events. This argument is also consistent with the correlation between geochemistry and mineralogy/textures in the Nushan xenoliths, which is different from those observed in the Lherz peridotites and in some other xenolith suites for which different metasomatic signatures are ascribed to a single event. For instance, Ionov *et al*. (2002) described two types of xenoliths from Spitzbergen. All enriched xenoliths with convex-upward REE patterns contain amphibole, whereas those with strongly fractionated LREE are generally amphibole free. A similar observation was made at Lherz, where the peridotites with flat REE patterns contain amphibole, whereas the enriched ones are devoid of this mineral (Bodinier *et al*., 1990).

However, the model involving two distinct metasomatic events cannot explain why melts of different compositions intruded different levels of the mantle. In other words, why were anhydrous veins produced only in the deeper part of the lithosphere, leaving the upper part unaffected, and why were hydrous veins confined to the shallower mantle? Cpx from Fe-rich

amphibole-free samples is isotopically very similar to that from the amphibole-peridotites (Table 3); thus the metasomatic agents involved in both suites may have a similar source. The isotopic similarity between metasomatized xenoliths and the Cenozoic basalts from eastern China (Fig. 7) further suggests an asthenospheric origin for the metasomatic agents. We thus suggest that the two metasomatic events recorded in the Nushan xenoliths may be genetically related. The different metasomatic assemblages and trace element signatures in the two groups can be accounted for, respectively, in terms of P–T control on phase stability and progressive chemical evolution of asthenosphere-derived melts during upward migration along channels or cracks.

The Nushan amphibole-peridotites equilibrated between 850 and 950°C, in contrast to the high temperature of the amphibole-free samples (990–1110°C). At a first sight, this picture is enigmatic because experiments show that amphibole is stable up to 1100°C and at pressures up to 30 kbar (Wallace & Green, 1991; Wyllie & Wolf, 1993). However, a literature survey reveals a predominant low equilibrium temperature (<1000°C) for amphibole-bearing (basalt-hosted) peridotites with only a few rare exceptions (e.g. Francis, 1976; Wilshire *et al.*, 1980; Witt & Seck, 1989; Vaselli *et al.*, 1995; Chazot *et al.*, 1996; Ionov *et al.*, 2002). Hence, the occurrence of amphibole in the lower-temperature regime in the mantle is real and needs an explanation. Figure 10a shows the relationships between the regional geotherm, peridotite solidus and experimentally determined stability field of amphibole. In the Nushan case, the mantle xenolith-derived geotherm corresponds to ~80 mW/m^2 (Xu *et al.*, 1998*a*) and cuts the wet solidus of peridotite at a relatively shallow level (~45 km; Fig. 10a). If the mantle xenoliths had equilibrated on the local geotherm, the amphibole-bearing and amphibole-free peridotites would have occupied different positions relative to the wet solidus. Whereas the former could have been situated below the wet solidus, the latter would have been located above the wet solidus, i.e. within the region of partial melting under hydrous conditions (shaded area in Fig. 10a). Although amphibole is stable in this shaded area, partial melting would rapidly consume hydrous phases because the latter have relatively lower melting points compared with other anhydrous minerals such as olivine and pyroxene. Moreover, in the lithospheric mantle, amphibole is expected to crystallize only where melt has infiltrated, as can be monitored by LREE and/or Fe enrichment (e.g. in wall-rocks). However, the wall-rocks were probably affected by transient heating while the dykes were emplaced. The thermal gradient in the vicinity of dykes may have been high enough to approach the amphibole-out reaction. These factors would significantly limit the formation of amphibole in the high-temperature regime (>1000°C) and confine the formation of amphibole to the low-temperature regime where the thermal gradient and wet solidus are not crossed. Another factor influencing the behaviour of amphibole formation is water activity in the melts concerned. In the lower lithospheric mantle, melt circulating in dykes may have been too primitive to have a high water content. As suggested by observations on orogenic peridotites (Woodland *et al.*, 1996; Bodinier *et al.*, 2004), it is possible that only evolved melts resulting from the segregation of anhydrous pyroxenites in dykes had a high water content, so that they could have precipitated amphibole at shallower levels.

A possible scenario in the Nushan case is proposed as follows. Partial melting of the asthenosphere formed melts that migrated upwards along melt channels or dykes as a result of their buoyancy. These melt fractions contained a small amount of water, but they did not crystallize amphibole in the lower part of the lithospheric mantle because of the high geothermal gradient and low water activity in the bulk system. Precipitation of olivine and pyroxene, or solidification of melts, resulted in the formation of essentially anhydrous veins/dykes, which acted as sources of metasomatism seen in the amphibole-free peridotites. Metasomatism is generally limited to areas adjacent to the dykes, probably because of the low content of volatiles in the melts. As a result of early crystallization of anhydrous mafic phases (i.e. pyroxenite), residual melts became enriched in water and the HIE, but depleted in the HFSE. These melts continued to migrate upward, crystallized amphibole and pervasively percolated a relatively large part of the shallow mantle. In this sense, although spatially separated, the metasomatic events that affected the Nushan xenoliths were temporally and genetically related and can be considered as a result of a single event.

The nature of the mantle beneath Nushan

The Sino-Korean Craton experienced widespread thermotectonic reactivation during the late Mesozoic, which resulted in destruction of the lithospheric keel (Menzies *et al.*, 1993; Griffin *et al.*, 1998). The removal of the lower part of the lithosphere was probably coeval with emplacement of hot asthenospheric material at the expense of the lower lithosphere, followed by slow thermal relaxation (Platt *et al.*, 1998). The current lithospheric mantle beneath eastern China is probably hybridized, with old lithosphere in the shallowest part and newly created 'oceanic' type lithosphere in the deeper part (e.g. Menzies *et al.*, 1993; Griffin *et al.*, 1998; Fan *et al.*, 2000; Xu, 2001). However, this model is difficult to test, largely because of the uncertainty

associated with dating of the lithospheric mantle (Gao *et al*., 2002; Zhi *et al*., 2002). All the Nushan peridotites have fertile to mildly depleted major element compositions. In our view, they are thus too fertile to be samples of the ancient cratonic mantle, which are invariably highly magnesian residues. Metasomatic assemblages and trace element signatures in the Nushan xenoliths are also significantly different from those in cratonic mantle (e.g. Menzies & Hawkesworth, 1987). Moreover, the isotope geochemistry of the amphibole-bearing peridotites resembles that of the Cenozoic basalts, which are believed to be derived from the asthenosphere (e.g. Liu *et al*., 1994; Zou *et al*., 2000). Accordingly, the Nushan peridotites can be interpreted as newly accreted lithosphere as a result of lithospheric thinning and subsequent thermal relaxation.

Nevertheless, some ambiguities associated with this simple accretion model need to be clarified, because (1) a few amphibole-free samples have ε_{Nd} as high as +11, out of the range of the Cenozoic basalts from eastern China (Fig. 7), and (2) this model cannot explain the different textures between the amphibole-bearing and amphibole-free peridotites. Previous studies have revealed an apparent correlation between texture and equilibrium temperature, with protogranular xenoliths commonly having higher temperatures than equigranular ones (Zangana *et al*., 1997, and references therein). This may result either from faster diffusional re-equilibration in smaller crystals or from enhanced mineral re-equilibration during recrystallization. However, the Nushan samples show the reverse relationship. Equilibration temperatures of amphibole-free peridotites, which have a predominant equigranular texture, are higher than those of amphibole-bearing xenoliths, of which most are characterized by coarse grains (Table 1).

Recent numerical modelling (Morency *et al*., 2002) demonstrates that lithospheric erosion is not a pure thermal process because the vertical extent of diffusive heat transport is too limited. To have efficient lithospheric thinning, very small-scale convection cells (not more than 10 km high) have to be involved (Morency *et al*., 2002). Upon thermal relaxation, the whole thermotectonic system at the lithosphere–asthenosphere boundary freezes, with the lower part of the lithosphere being composed of a mixture of eroded lithospheric peridotites and materials from the convective mantle. The thermotectonic evolution in eastern China at the transition between late Mesozoic and early Cenozoic can be viewed in a similar way (Xu, 2001). It is therefore not surprising to find a lithospheric signature in newly accreted lithosphere.

The amphibole-free peridotites could represent samples of the lower layer of newly accreted lithosphere. Although locally preserving a lithospheric signature, the materials in this layer were probably heated during small-scale convection, partially melted and deformed at high temperature. The amphibole-peridotites might represent samples of the upper part of the accreted lithosphere, in which small-scale convection was not significant. Perhaps it is this less efficient heat transportation that resulted in the coarse-grained texture typical of the amphibole-bearing samples. Both suites were then subjected to cooling as a result of general thermal decay in the Cenozoic (Menzies & Xu, 1998). The amphibole-free peridotites completely re-equilibrated, probably because of efficient diffusion at relatively high temperature, enhanced by dynamic recrystallization. In contrast, the amphibole-peridotites were undergoing re-equilibration at the time of eruption of the host basalts. Metasomatism probably took place during thermal relaxation, as the decoupling between high LREE/HREE ratios and depleted isotopic compositions precludes an older event.

ACKNOWLEDGEMENTS

We thank C. Y. Lin, J.-C. Mercier and B. Orberger for their help in the field, and M. Fialin, S. Pourtales, M. Godard and M. Thirlwall for technical assistance. H. Downes, D. Ionov, E.-R. Neumann and G. Yaxley are thanked for their careful and constructive reviews, which substantially improved the paper. Financial support from the China National Natural Science Foundation (49925308, 49703042), the Ministry of Science and Technology (pre-selected 39 project) and INSU-CNRS of France are gratefully acknowledged. This paper results from an international co-operation project between CAS (China) and CNRS (France).

REFERENCES

Baker, L. & Haggerty, S. E. (1967). The alteration of olivine in basalts and associated lavas. *Contributions to Mineralogy and Petrology* **16**, 233–273.

Basu, A. R., Wang, J. W., Huang, W. K., Xie, G. H. & Tatsumoto, M. (1991). Major element, REE and Pb, Nd and Sr isotopic geochemistry of Cenozoic volcanic rocks of eastern China: implications for origin from suboceanic-type mantle reservoirs. *Earth and Planetary Science Letters* **105**, 149–169.

Bedini, R. M. & Bodinier, J.-L. (1999). Distribution of incompatible trace elements between the constituents of spinel peridotite xenoliths: ICP-MS data from the East African Rift. *Geochimica et Cosmochimica Acta* **63**, 3883–3900.

Bedini, R. M., Bodinier, J.-L., Dautria, J. M. & Morten, L. (1997). Evolution of LILE-enriched small melt fractions in the lithospheric mantle: a case study from the Eastern African Rift. *Earth and Planetary Science Letters* **153**, 67–83.

Bodinier, J.-L., Vasseur, G., Vernières, J., Dupuy, C. & Fabriès, J. (1990). Mechanisms of mantle metasomatism: geochemical evidence from the Lherz orogenic peridotite. *Journal of Petrology* **31**, 597–628.

Bodinier, J.-L., Merlet, C., Bedini, R. M., Simien, F., Remaid, R. & Carrido, C. J. (1996). The distribution of niobium, tantalum, and other highly incompatible trace elements in the lithospheric mantle: the spinel paradox. *Geochimica et Cosmochimica Acta* **60**, 545–550.

Bodinier, J.-L., Menzies, M. A., Shimizu, N., Frey, F. A. & McPherson, E. (2004). Hydrous, silicate and carbonate metasomatism at Lherz, France: contemporaneous derivatives of silicate melt–harzburgite reaction. *Journal of Petrology* **45**, 299–320.

Brey, G. P. & Kohler, T. (1990). Geothermobarometry in four-phase lherzolites II. New thermobarometers, and practical assessment of existing thermobarometers. *Journal of Petrology* **31**, 1353–1378.

Cabanes, N. & Mercier, J.-C. C. (1988). Insight into the upper mantle beneath an active extensional zone: the spinel-peridotite xenoliths from San Quintin (Baja California, Mexico). *Contributions to Mineralogy and Petrology* **100**, 374–382.

Chazot, G., Menzies, M. & Harte, B. (1996). Determination of partition coefficients between apatite, clinopyroxene, amphibole, and melt in natural spinel lherzolite from Yemen: implications for wet melting of the lithospheric mantle. *Geochimica et Cosmochimica Acta* **60**, 423–437.

Chen, G. Y., Song, Z. H., An, C. Q., Cheng, L. H., Zhuang, Z., Fu, Z. W., Lu, Z. L. & Hu, J. F. (1991). Three dimensional crust and upper mantle structure of the North China region. *Acta Geophysica Sinica* **34**, 172–181 (in Chinese).

Dick, H. J. B. & Bullen, T. (1984). Chromian spinel as a petrogenetic indicator in abyssal and alpine-type peridotites and spatially associated lavas. *Contributions to Mineralogy and Petrology* **86**, 54–76.

E, M. L. & Zhao, D. S. (eds) (1987). *Cenozoic Basalts and their Deep-seated Inclusions, Eastern China*. Beijing: Scientific Press, 490 pp.

Eggins, E. M., Rudnick, R. L. & McDonough, W. F. (1998). The composition of peridotites and their minerals: a laser-ablation ICP-MS study. *Earth and Planetary Science Letters* **154**, 53–71.

Fan, W. M., Zhang, H. F., Baker, J., Jarvis, K. E., Mason, P. R. D. & Menzies, M. A. (2000). On and off the North China Craton: where is the Archaean keel? *Journal of Petrology* **41**, 933–950.

Francis, D. M. (1976). The origin of amphibole in lherzolite xenoliths from Nunivak Island, Alaska. *Journal of Petrology* **17**, 357–378.

Gao, S., Rudnick, R. L., Carlson, R. W., McDonough, W. & Liu, Y. S. (2002). Re–Os evidence for replacement of ancient mantle lithosphere beneath the North China Craton. *Earth and Planetary Science Letters* **198**, 307–322.

Griffin, W. L., Zhang, A. D., O'Reilly, S. Y. & Ryan, G. (1998). Phanerozoic evolution of the lithosphere beneath the Sino-Korean Craton. In: Flower, M., Chung, S. L., Lo, C. H. & Lee, T. Y. (eds) *Mantle Dynamics and Plate Interactions in East Asia*. *American Geophysical Union Geodynamic Series* **27**, 107–126.

Hart, S. R. & Dunn, T. (1993). Experimental cpx/melt partitioning of 24 trace elements. *Contributions to Mineralogy and Petrology* **113**, 1–8.

Hauri, E. H., Wagner, T. P. & Grove, T. L. (1994). Experimental and natural partitioning of Th, U, Pb and other elements between garnet, clinopyroxene and basaltic melts. *Chemical Geology* **117**, 149–166.

Ionov, D. A. & Hofmann, A. W. (1995). Nb–Ta-rich mantle amphiboles and micas: implications for subduction-related metasomatic trace element fractionations. *Earth and Planetary Science Letters* **131**, 341–356.

Ionov, D. A., Savoyant, L. & Dupuy, C. (1992). Application of the ICP-MS technique to trace element analysis of peridotites and their minerals. *Geostandard Newsletters* **16**, 311–315.

Ionov, D. A., Dupuy, C., O'Reilly, S. Y., Kopylova, M. G. & Genshaft, Y. S. (1993). Carbonated peridotite xenoliths from Spitsbergen: implications for trace element signature of mantle carbonate metasomatism. *Earth and Planetary Science Letters* **119**, 283–297.

Ionov, D., Bodinier, J.-L., Mukasa, S. B. & Zanetti, A. (2002). Mechanisms and sources of mantle metasomatism: major and trace element compositions of peridotite xenoliths from Spitsbergen in the context of numerical modeling. *Journal of Petrology* **43**, 2219–2259.

Jaques, A. L. & Green, D. H. (1980). Anhydrous melting of peridotite at 0–15 kb pressure and the genesis of tholeiitic basalt. *Contributions to Mineralogy and Petrology* **73**, 287–310.

Kalfoun, F., Ionov, D. A. & Merlet, C. (2002). HFSE residence and Nb–Ta ratios in metasomatised, rutile-bearing mantle peridotites. *Earth and Planetary Science Letters* **199**, 49–65.

Kelemen, P. B., Whitehead, J. A., Aharonov, E. & Jordahl, K. A. (1995). Experiments on flow focusing in soluble porous media, with application to melt extraction from the mantle. *Journal of Geophysical Research* **100**, 475–496.

Kempton, P. D. (1987). Mineralogic and geochemical evidence for differing styles of metasomatism in spinel lherzolite xenoliths: enriched mantle source regions of basalts. In: Menzies, M. & Hawkesworth, C. J. (eds) *Mantle Metasomatism*. New York: Academic Press, pp. 45–89.

Liu, C. Q., Masuda, A. & Xie, G. H. (1994). Major- and trace-element compositions of Cenozoic basalts in eastern China: petrogenesis and mantle source. *Chemical Geology* **114**, 19–42.

McKenzie, D. P. (1989). Some remarks on the movement of small melt fractions in the mantle. *Earth and Planetary Science Letters* **95**, 53–72.

Menzies, M. A. & Hawkesworth, C. J. (1987). *Mantle Metasomatism*. New York: Academic Press.

Menzies, M. A. & Xu, Y. G. (1998). Geodynamics of the North China Craton. In: Flower, M., Chung, S. L., Lo, C. H. & Lee, T. Y. (eds) *Mantle Dynamics and Plate Interactions in East Asia*. *American Geophysical Union Geodynamic Series* **27**, 155–165.

Menzies, M. A., Kempton, P. D. & Dungan, M. (1985). Interaction of continental lithosphere and asthenospheric melts below the Geronimo Volcanic Field, Arizona, U.S.A. *Journal of Petrology* **26**, 663–693.

Menzies, M. A., Fan, W. M. & Zhang, M. (1993). Palaeozoic and Cenozoic lithoprobes and the loss of >120 km of Archaean lithosphere, Sino-Korean craton, China. In: Prichard, H. M., Alabaster, T., Harris, N. B. W. & Neary, C. R. (eds) *Magmatic Processes and Plate Tectonics*. *Geological Society, London, Special Publications* **76**, 71–78.

Mercier, J.-C. & Nicolas, A. (1975). Textures and fabrics of upper mantle peridotites as illustrated by xenoliths from basalts. *Journal of Petrology* **16**, 454–487.

Morency, C., Doin, M.-P. & Dumoulin, C. (2002). Convective destabilization of a thickened continental lithosphere. *Earth and Planetary Science Letters* **202**, 303–320.

Navon, O. & Stolper, E. (1987). Geochemical consequence of melt percolation: the upper mantle as a chromatographic column. *Journal of Geology* **95**, 285–307.

Peng, Z. C., Zartman, R. E., Futa, E. & Chen, D. G. (1986). Pb-, Sr- and Nd-isotopic systematics and chemical characteristics of Cenozoic basalts, eastern China. *Chemical Geology* **59**, 3–33.

Platt, J. P., Soto, J. I., Whitehouse, M. J., Hurford, A. J. & Kelley, S. P. (1998). Thermal evolution, rate of exhumation, and tectonic significance of metamorphic rocks from the floor of the Alboran extensional basin, Western Mediterranean. *Tectonics* **17**, 671–689.

Preß, S., Witt, G., Seck, H. A., Ionov, D. & Kovalenko, V. I. (1986). Spinel peridotite xenoliths from the Tariat Depression, Mongolia. I: Major element chemistry and mineralogy of a primitive mantle xenolith suite. *Geochimica et Cosmochimica Acta* **50**, 2587–2599.

Sautter, V., Jaoul, O. & Abei, F. (1988). Aluminium diffusion in diopside using the ^{27}Al (p,r) ^{28}Si nuclear reaction: preliminary results. *Earth and Planetary Science Letters* **79**, 169–186.

Schneider, M. E. & Eggler, D. H. (1986). Fluids in equilibrium with peridotite minerals: implications for mantle metasomatism. *Geochimica et Cosmochimica Acta* **50**, 711–724.

Song, Y., Frey, F. A. & Zhi, X. (1990). Isotopic characteristics of Hannuoba basalts, eastern China: implications for their petrogenesis and the composition of subcontinental mantle. *Chemical Geology* **85**, 35–52.

Sun, S.-S. & McDonough, W. F. (1989). Chemical and isotopic systematics of oceanic basalts: implications for mantle composition and processes. In: Saunders, A. D. & Norry, M. J. (eds) *Magmatism in the Ocean Basins*. *Geological Society, London, Special Publications* **42**, 313–345.

Thirlwall, M. F. (1991). Long-term reproducibility of multicollector Sr and Nd isotope ratio analysis. *Chemical Geology* **94**, 85–104.

Tiepolo, M., Bottazzi, P., Foley, S., Oberti, R., Vannucci, R. & Zanetti, A. (2001). Fractionation of Nb and Ta from Zr and Hf at mantle depths: the role of titanian paragasite and kaersutite. *Journal of Petrology* **42**, 221–232.

Vaselli, O., Downes, H., Thirlwall, M., Dobosi, G., Coradossi, N., Seghedi, I., Szakacs, A. & Vannucci, R. (1995). Ultramafic xenoliths in Plio-Pleistocene alkali basalts from the Eastern Transylvanian bsasin: depleted mantle enriched by vein metasomatism. *Journal of Petrology* **36**, 23–53.

Vernières, J., Godard, M. & Bodinier, J.-L. (1997). A plate model for the simulation of trace element fractionation during partial melting and magmas transport in the Earth's upper mantle. *Journal of Geophysical Research* **102**, 24771–24784.

Wallace, M. E. & Green, D. H. (1991). The effect of bulk compositions on the stability of amphibole in the upper mantle: implications for solidus positions and mantle metasomatism. *Petrology and Mineralogy* **44**, 1–9.

Werling, F. & Altherr, R. (1997). Thermal evolution of the lithosphere beneath the French Massif Central as deduced from geothermobarometry on mantle xenoliths. *Tectonophysics* **275**, 119–141.

Wilkinson, J. F. G. & Le Maitre, R. W. (1987). Upper mantle amphiboles and micas and TiO_2, K_2O, and P_2O_5 abundances and 100 $Mg/(Mg + Fe^{2+})$ ratios of common basalts and andesites: implications for modal metasomatism and undepleted mantle compositions. *Journal of Petrology* **28**, 37–73.

Wilshire, H. G., Nielson Pike, J. E., Meyer, C. E. & Schwarzman, Z. C. (1980). Amphibole-rich veins in lherzolite xenoliths, Dish Hill, and Deadman Lake, California. *American Journal of Sciences* **280A**, 576–593.

Witt, G. E. & Seck, H. A. (1987). Temperature history of sheared mantle xenoliths from the west Eifel, West Germany: evidence for mantle diapirism beneath the Rhenish Massif. *Journal of Petrology* **28**, 475–493.

Witt, G. E. & Seck, H. A. (1989). Origin of amphibole in recrystallized and porphyroclastic mantle xenoliths from the Rhenish Massif: implications for the nature of mantle metasomatism. *Earth and Planetary Science Letters* **91**, 327–340.

Witt-Eickschen, G. E. & Seck, H. A. (1991). Solubility of Ca and Al in orthopyroxene from spinel peridotite: an improved version of an empirical geothermometer. *Contributions to Mineralogy and Petrology* **106**, 431–439.

Witt-Eickschen, G. E., Seck, H. A. & Reys, C. (1993). Multiple enrichment processes and their relationships in the subcrustal lithosphere beneath the Eifel (Germany). *Journal of Petrology* **34**, 1–22.

Woodland, A. B., Kornprobst, J., McPherson, E., Bodinier, J.-L. & Menzies, M. A. (1996). Metasomatic interactions in the lithospheric mantle: petrologic evidence from the Lherz massif, French Pyrenees. *Chemical Geology* **134**, 83–112.

Wyllie, P. J. & Wolf, M. B. (1993). Amphibolite dehydration-melting: sorting out the solidus. In: Prichard, T. M., Alabaster, T., Harris, N. B. W. & Neary, C. R. (eds) *Magmatic Processes and Plate Tectonics*. *Geological Society, London, Special Publications* **76**, 405–416.

Xu, Y. G. (2001). Thermo-tectonic destruction of the Archaean lithospheric keel beneath eastern China: evidence, timing and mechanism. *Physics and Chemistry of the Earth (A)* **26**, 747–757.

Xu, Y. G., Ross, J. V. & Mercier, J.-C. (1993). The upper mantle beneath the continental rift of Tanlu, Eastern China: evidence for the intralithospheric shear zones. *Tectonophysics* **225**, 337–360.

Xu, Y. G., Mercier, J.-C. & Lin, C. Y. (1997). Amphibole-bearing peridotite xenoliths from Nushan, Anhui Province: evidence for melt percolation process in the upper mantle and lithospheric uplift. *Chinese Journal of Geochemistry* **16**, 213–229.

Xu, X. S., O'Reilly, S. Y., Griffin, W. L. & Zhou, X. M. (1998*a*). The nature of the Cenozoic lithosphere at Nushan, Central Eastern China. In: Flower, M., Chung, S. L., Lo, C. H. & Lee, T. Y. (eds) *Mantle Dynamics and Plate Interactions in East Asia*. *American Geophysical Union Geodynamic Series* **27**, 167–195.

Xu, Y. G., Menzies, M. A., Vroon, P., Mercier, J. C. C. & Lin, C. Y. (1998*b*). Texture–temperature–geochemistry relationship in the upper mantle as revealed from spinel peridotite xenoliths from Wangqing, NE China. *Journal of Petrology* **39**, 469–493.

Xu, Y. G., Menzies, M. A., Bodinier, J.-L., Bedini, R. M., Vroon, P. & Mercier, J.-C. (1998*c*). Melt percolation–reaction atop the plume: evidence from poikiloblastic spinel harzburgite xenoliths from Boree (Massif Central, France). *Contributions to Mineralogy and Petrology* **132**, 65–84.

Xu, X. S., O'Reilly, S. Y., Griffin, W. L. & Zhou, X. M. (2000). Genesis of young lithospheric mantle in the southeastern China: a LAM-ICPMS trace element study. *Journal of Petrology* **41**, 111–148.

Zangana, N. A., Downes, H., Thirlwall, M. F. & Hegner, L. (1997). Relationship between deformation, equilibration temperatures, REE and radiogenic isotopes in mantle xenoliths (Ray Pic, Massif Central, France): an example of plume–lithosphere interaction? *Contributions to Mineralogy and Petrology* **127**, 187–203.

Zhang, R. Y. & Cong, B. L. (1987). Cenozoic volcanic rocks and its xenoliths from southeastern China. In: E, M. L. & Zhao, D. S. (eds) *Cenozoic Basalts and their Deep-seated Inclusions, Eastern China*. Beijing: Scientific Press, pp. 349–467 (in Chinese).

Zhi, X. C., Reisberg, L., Wagner, C., Peng, Z. C. & Xu, X. S. (2002). Longevity and multistage evolution of subcontinental lithospheric mantle beneath eastern China: evidence from Re–Os isotope geochemistry of mantle peridotite xenoliths from Jiangsu and Anhui Provinces, China. *Geochimica et Cosmochimica Acta* **66**(15A), A876.

Zindler, A. & Hart, S. R. (1986). Chemical geodynamics. *Annual Review of Earth and Planetary Sciences* **14**, 493–571.

Zou, H. B., Zindler, A., Xu, X. S. & Qi, Q. (2000). Major, trace element, and Nd, Sr and Pb isotope studies of Cenozoic basalts in SE China: mantle sources, regional variations and tectonic significance. *Chemical Geology* **171**, 33–47.